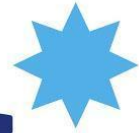




H2020 - Research and Innovation Action

APPLICATE^{*}



**Advanced Prediction in Polar regions and beyond: Modelling, observing system design and Linkages associated with a Changing Arctic climaTE
Grant Agreement No: 727862**

Deliverable No. 2.3
**Recommendations on the inclusion of APPLICATE
model enhancements in NWP models**

Submission of Deliverable

Work Package	WP2 Enhanced weather and climate models
Deliverable No	2.3
Deliverable title	Recommendations on the inclusion of APPLICATE model enhancements in NWP models
Version	v1
Status	Final
Dissemination level	CO - Confidential, only for members of the consortium
Lead Beneficiary	Select
Contributors	<input type="checkbox"/> 1 – AWI <input type="checkbox"/> 2 – BSC X 3 - ECMWF <input type="checkbox"/> 4 – UiB <input type="checkbox"/> 5 – UNI Research <input type="checkbox"/> 6 – MET Norway <input type="checkbox"/> 7 – Met Office <input type="checkbox"/> 8 – UCL <input type="checkbox"/> 9 - UREAD X 10 – SU X 11 – CNRS-GAME <input type="checkbox"/> 12 - CERFACS <input type="checkbox"/> 13 – AP <input type="checkbox"/> 14 – UiT <input type="checkbox"/> 15 - IORAS <input type="checkbox"/> 16 - MGO
Due Date	31/10/2019
Delivery Date	31/10/2019
Coordinating author	D. Salas y Mélia, CNRS-GAME, david.salas@meteo.fr
Contributing authors	N. Azouz, V. Guémas, A. Napoly, E. Bazile (CNRS-GAME), I. Sandu, G. Arduini (ECMWF), A. Fitch (SU)



This project has received funding from the European Union's Horizon 2020 Research & Innovation programme under grant agreement No. 727862.

Table of Contents

EXECUTIVE SUMMARY	4
1. INTRODUCTION	5
1.1. Background and objectives	5
1.2. Organisation of this report	9
2. METHODOLOGY	9
3. RESULTS AND DISCUSSION	21
4. CONCLUSIONS AND OUTLOOK	32
5. REFERENCES	35

EXECUTIVE SUMMARY

This deliverable provides an assessment of the impact of new and/or improved model components developed within APPLICATE WP2 into numerical weather prediction (NWP) systems. Based on these conclusions, it provides recommendations about priorities to pursue for further model developments and components to include in the next generation of NWP systems.

The APPLICATE developments considered in this deliverable are:

- the inclusion of dynamical and/or thermodynamic sea ice models.
- the extension of single-layer snow schemes on land to multi-layer snow schemes.
- the inclusion of snow schemes on top of sea ice.
- an improved version of the eddy-diffusivity mass-flux scheme which detects decoupled stratocumulus.

Introducing an interactive sea ice model into numerical weather predictions leads to a robust increase in forecast quality for near-surface temperature close to the sea ice edge in the ARPEGE/AROME prediction system. Both bias and standard deviation are substantially reduced. The temperature gradient across the sea ice edge is more realistic. Exploiting both observed sea surface temperatures and sea ice fraction to initialize the model is essential to optimize the benefits from the interactive sea ice model. Similarly, extracting boundary conditions from a global model which also uses an interactive sea ice model improves substantially the performance of the regional prediction system. The dynamic coupling of the ice cover in IFS allows for capturing accurately rapid changes in sea ice concentration, especially along the sea ice edge as illustrated on a case study. A substantial impact is seen in the near surface temperature (up to 6°C) when the large-scale meteorological situation is favourable.

At high latitudes, near-surface temperature tends to be overestimated during cold events occurring in clear-sky conditions. Introducing a multi-layer snow scheme over land into the IFS prediction systems leads to a better representation of these cold events at forecast day 2 over the Sodankylä observational supersite. The diurnal cycle in near surface temperature is also better captured with the multi-layer snow scheme than with the previous single-layer scheme, with a reduced warm bias at the daily minimum and cold bias at the daily maximum.

Including this multi-layer snow scheme over sea ice allows for a marginally better simulated temperature in the lower atmosphere for a case study from the SHEBA campaign. However, during periods of liquid-phase cloud cover, systematic errors in the representation of such clouds leads to the increase of the errors of skin temperature in the simulation using the multi-layer snow scheme. These results highlight the key role of compensating errors in the surface energy balance and the need for improved representation of Arctic boundary layer processes.

A revised version of the eddy-diffusivity mass-flux scheme was proposed to identify decoupled stratocumulus. This scheme detects and simulates cloud layers that would not have been represented before, as seen in an ASCOS Arctic stratocumulus case. The root mean square error for clouds and radiative properties are drastically reduced with this improved scheme.

1. INTRODUCTION

1.1. Background and objectives

In this report, we describe the implementation and evaluation of the main model enhancements developed in WP2 and their impact on weather forecasts in the Arctic. The two numerical weather prediction systems used are IFS and ARPEGE/AROME developed and operated by ECMWF and Météo-France, respectively. Please note that part of the material reported in this document is reproduced from Arduini et al. (2019), Keeley and Mogensen (2018) and Voldoire et al. (2019), where extra information can be found.

1.1.1. Sea ice

Sea ice is a major component of the climate system, because of its influence on surface fluxes, especially when the overlying atmosphere is much colder than the ocean, as it is usually the case in the Arctic during winter. Fluxes can be several hundreds of watts per square metre over open-water and approach zero over thick, snow-covered ice. Open water provides a local heat source which has the potential to alter the local as well as the wider meteorological situation. Some climate models include a sea ice component since the 1990s, whereas they have been only recently added to NWP systems for weather forecasts. In the past, sea ice fields were assumed to change so slowly that it was acceptable to keep them fixed for the period covered by global medium-range forecasts.

Following this assumption, in the current ARPEGE forecast system used operationally, the fraction and surface temperature of sea ice are respectively initialised depending on sea-surface temperature and from a climatology. During the forecast, sea ice fraction and surface temperature are kept at their initial values. At the beginning of APPLICATE, sea ice was also held fixed in the ECMWF medium-range deterministic ten-day forecasts (HRES). During APPLICATE, a dynamical sea ice model was introduced in the ECMWF HRES forecasts, and a thermodynamic model was included in the AROME/ARPEGE forecast system, the details of which are discussed in section 2.1.1. Although it is acceptable to fix the sea ice over the length of a forecast for a few days at the heart of the pack ice (excluding strong sea ice deformation events), it is not justified in regions close to the ice edge, where there is often rapid growth or melt. Indeed, variations in sea ice coverage can be important close to the ice edge at typical NWP time scales (from 1 to 10 days) (see Figure 1.1). In the Northern Hemisphere (NH) during the period between June to November, significant variations of sea ice coverage occur in more than 10% of the total ice field. In the Southern Hemisphere (SH), these variations can be even larger during the summer months, demonstrating the need of an interactive sea ice cover for NWP applications.

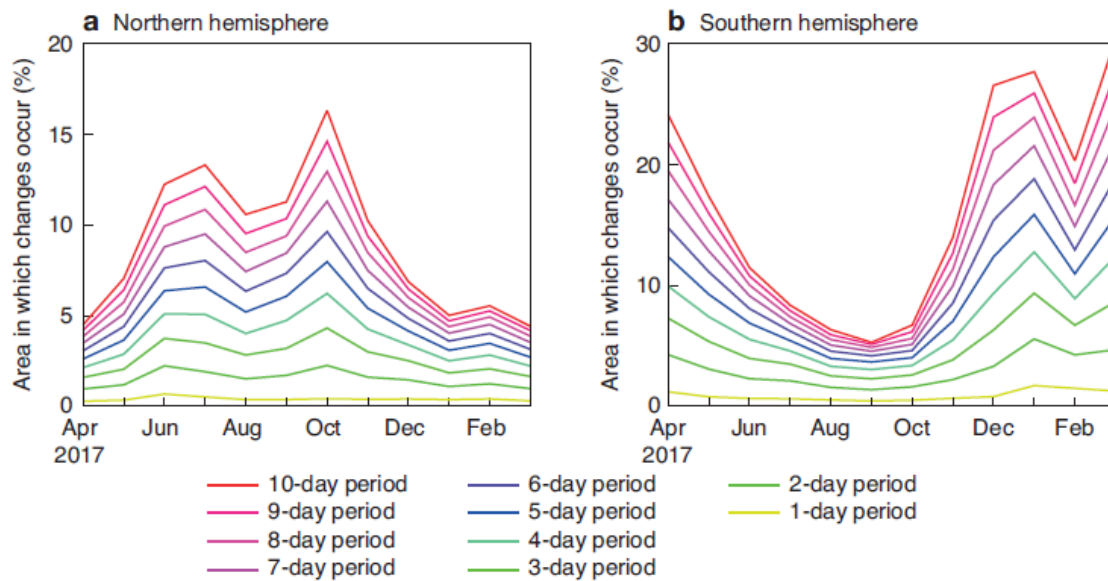


Figure 1.1: Monthly-mean percentage of the sea ice field in which significant changes in sea ice concentration (>15%) occur over different periods of time, based on OCEAN5 analysis fields for April 2017 to March 2018, for (a) the northern hemisphere and (b) the southern hemisphere (taken from Keeley and Mogensen, 2018).

1.1.2. Snow on land

NWP systems used for weather forecasts and reanalysis traditionally use single-layer snow schemes to describe the snowpack (Balsamo et al., 2015; Dee et al., 2011; Dutra et al., 2010). These consist of an additional layer of snow on top of the soil layers, using physical or empirical parameterizations of snow processes to represent the temporal evolution of the snowpack. A main limitation of such schemes is that they can only represent the temporal evolution of snow processes on a single time-scale, implying that processes taking place on a range of time-scales from (sub) diurnal to seasonal cannot be properly represented (see for instance Jin et al., 1999). This affects the correct simulation of snow depth and cover during accumulation and ablation periods, also impacting on soil freezing and hydrological cycle (Dutra et al., 2012; Saha et al., 2017).

The snowpack representation is also important for other surface components, like soil temperature and moisture. A more realistic description of the snowpack vertical density and temperature gradients enables a better description of heat fluxes across the snow-soil interface, reducing persistent biases in wintertime soil temperature over the Siberian region (Burke et al., 2013; Decharme et al., 2016; Dutra et al., 2012), with implications for changes in the permafrost extension in climate change sensitivity studies (Burke et al., 2013). A realistic representation of the thermal insulation properties of the snowpack also improves the energy (heat) coupling with the atmosphere, with a positive impact on wintertime near-surface temperature biases of climate models over snow-covered regions (Dutra et al., 2012; Saha et al., 2017).

NWP systems have difficulties to correctly represent the diurnal cycle of near-surface fields such as temperature and winds (see Haiden et al., 2018; Holtslag et al., 2013). As an example, the ECMWF IFS model shows a persistent (across years) warm bias of night-time minimum temperature at high-latitude regions during winter-time (see Figure 1.2). For the Scandinavian region, Haiden et al. (2018) showed that one of the key factors contributing to such biases is related to the modelling of the deep snowpack in the current version of IFS. In clear-sky nights, the top snow layer cools rapidly as a result of longwave radiative heat loss of the surface and the reduced heat input from the ground underneath because of the snow insulation properties. The correct representation of these processes is challenging for NWP systems using a single-layer snow scheme, because of the large thermal inertia associated

with a deep snowpack. Therefore, the implementation of multi-layer snow schemes is a foreseen solution for a more realistic snow-atmosphere coupling.

During APPLICATE, a new multi-layer snowpack scheme for land surfaces has been developed and evaluated within the ECMWF (IFS) prediction system, the details of which are discussed in section 2.2.

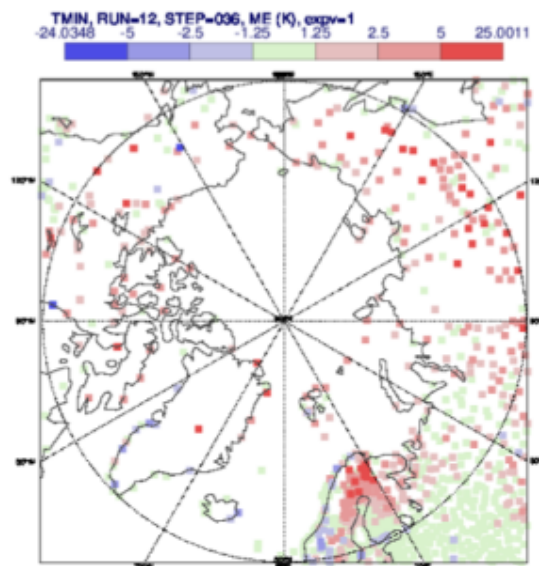


Figure 1.2: Bias of daily minimum 2-metre temperature of the ECMWF operational forecast in the second day of the forecast for DJF 2017 compared to SYNOP observations.

1.1.3. Snow on ice

Another aspect that is usually poorly represented in NWP systems is the effect of snow over sea ice surfaces. The presence of snow leads to an effective thermal decoupling between the ice and the atmosphere above during wintertime, reducing the heat transfer between the two media and therefore limiting the sea ice growth. During summertime, the formation of ponds due to the snow melting can increase the pace at which sea ice melts via a reduction of the surface albedo, which increases the solar radiation absorption.

The current ECMWF IFS prediction system does not simulate snow over sea ice. Therefore, when snow is present but not simulated, the ice temperatures are too warm in the IFS as the missing insulating effect of snow partly compensates for the surface radiative cooling. An example of this effect is shown in Figure 1.3 from the SHEBA campaign in early January 1998. The skin temperature in the IFS model (representing bare ice) is too warm compared to that observed (representing the top of snow layer). In reality, during clear sky events, the surface can cool rapidly due to the presence of snow, while the IFS has a limited capacity to represent this rapid cooling. Indeed, snow is a much better insulator than sea ice, and therefore, since snow over sea ice is not simulated in IFS, the insulating effect of the sea ice/snow slab is underestimated, therefore leading to the overestimation of the vertical heat diffusion from the underlying ocean towards the ice surface, which helps to maintain warmer temperatures at the surface. In cloudy conditions, the results are more complex to interpret. The model skin temperature is often cooler than the observed skin temperature, which could be due to the lack of snow layer but also to the ability of the model to produce clouds or to correctly partition liquid and ice water content within the clouds. This highlights the need for the model to capture both the snow/sea ice surface processes and the cloud cover/structure to correctly reproduce the surface temperatures. During APPLICATE, the multi-layer snow scheme developed and tested for land has also been tested over the sea ice in the HRES prediction system.

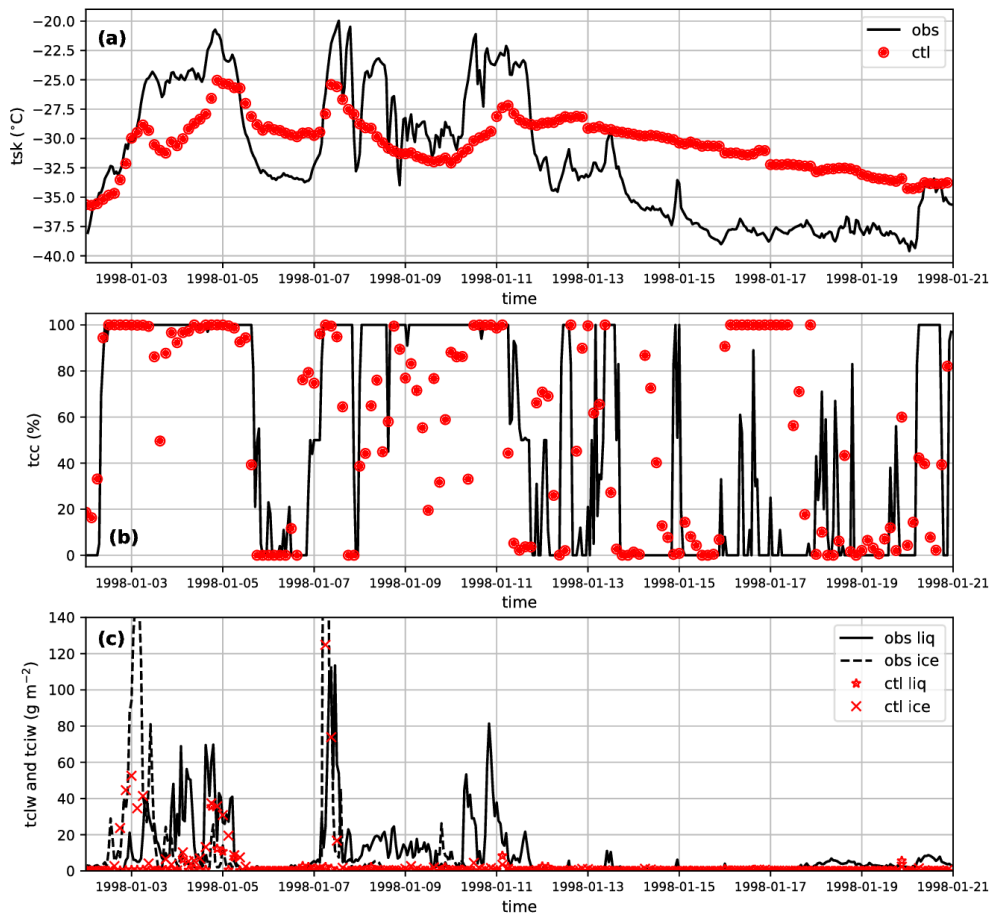


Figure 1.3: SHEBA observational data (obs, line) and model forecast for the nearest grid point (ctl, symbol). Showing skin temperature (top), total cloud cover (middle) and total column liquid and ice water (bottom).

1.1.4. Arctic atmospheric boundary layer

At present, the turbulent mixing in unstable boundary layers is represented in the IFS model using the eddy-diffusivity mass-flux (EDMF) method (Kohler et al. 2011). This approach involves two components to treat turbulent mixing depending on the scale of the turbulent eddies. Small eddies are treated as a K-diffusion component, which transport purely down-gradient. On the other hand, the largest and most energetic eddies are treated by a mass-flux component.

The most prevalent type of cloud in the Arctic is stratocumulus. An essential component of stratocumulus cloud dynamics is turbulent mixing driven by cloud-top radiative cooling. For unstable well-mixed stratocumulus-topped boundary layers, this process is represented in IFS through an additional K-diffusion component, proportional to the cloud-top radiative cooling. The total eddy diffusion coefficients for an unstable stratocumulus topped boundary layer are thus the sum of a surface and cloud-top driven eddy-diffusivity profile. At the top of the boundary layer these coefficients may be substituted with explicit entrainment. An entraining/detraining bulk plume model is used to determine the cloud base, cloud and boundary layer top in cases when the boundary layer is unstable (positive surface flux). The top of the boundary layer is defined as the height where the vertical velocity of the updraft air parcel drops to zero. The cloud base is defined as the lowest level where condensation occurs.

SU has tested a better representation of turbulent mixing in Arctic boundary layers in the ECMWF Integrated Forecasting System (IFS), the details of which are given in section 2.1.4.

1.1.5. Tasks

Task 1: As part of the Task 2.1.3 of APPLICATE, the GELATO-1d sea ice model (1d version of GELATO 6, used in the CNRM-CM6-1 coupled climate system, Voltaire et al., 2019) was activated in the ARPEGE/AROME NWP system and the LIM2 sea ice model was introduced in the ECMWF HRES forecasts. In this deliverable, we illustrate the benefits resulting from the activation of the GELATO-1d and LIM2 sea ice models respectively within the ARPEGE and AROME (GELATO, section 3.1) and the IFS (LIM, section 3.2) prediction systems.

Task 2: As part of the Task 2.1.2 of APPLICATE, a new multilayer snowpack scheme was developed and evaluated into the ECMWF IFS. In this deliverable, the performance of this new scheme is assessed both in offline and coupled simulations. The impact on snow processes was evaluated (i) using the in-situ observations of the Earth System Model Snow Intercomparison Project (ESM-SnowMIP, Krinner et al., 2018), (ii) global offline simulations evaluated against in-situ snow depth observations from the global SYNOP network and (iii) coupled IFS ten-days forecasts (section 3.3).

Task 3: As part of the Task 2.1.2 of APPLICATE, the multi-layer snow scheme developed over land was activated over sea ice and evaluated in the IFS prediction system, which at present does not consider snow over sea ice, in coupled weather forecasts. In this deliverable, the impact of the snow schemes was assessed in a prediction context in section 3.4.

Task 4: As part of the Task 2.1.1 of APPLICATE, a better representation of Arctic decoupled stratocumulus-topped boundary layers, as detailed in section 2.4, was tested in the ECMWF Integrated Forecasting System (IFS). In this deliverable, the added-value of this new representation is illustrated in section 3.5.

1.2. Organisation of this report

Section 2 of the report provides more details about each enhancement of the IFS and ARPEGE/AROME forecast systems that were considered for this report, the experimental protocols and the methodology used for their assessment. The benefits of including new components in IFS and ARPEGE/AROME on the forecast quality are presented in Section 3. Section 4 contains some concluding remarks and makes recommendations regarding model enhancements for improved NWP systems.

2. METHODOLOGY

2.1. New components

2.1.1. Sea ice

Sea ice in ARPEGE and AROME (CNRS-GAME)

The ARPEGE and AROME NWP models share the same land-surface platform SURFEX v8 (Le Moigne et al., 2018). Since SURFEX v8 is one-dimensional, the different sea ice schemes available in this model are one-dimensional as well. In order to test the added-value of an interactive sea ice model in a numerical weather prediction framework, we chose to use GELATO-1d, which is the 1d version of GELATO 6, the sea ice component of the CNRM-CM6-1 global coupled climate model (Voltaire et al., 2019). In GELATO-1d, all the horizontal processes represented in GELATO 6, namely dynamics and advection, are disabled. GELATO has an ice thickness distribution model (Salas y Melia, 2002), but for the tests presented in this document, only one category is considered. Hence within every grid cell, sea ice is represented by a single sea ice slab. The ice slab is vertically discretized into 9 vertical layers with equal thickness, and the snowpack that may cover sea ice is represented by a single additional layer. The sea ice enthalpy formulation is based on Notz (2005). As in Hunke and Lipscomb (2010), an

iterative method is used to solve the vertical heat diffusion equation in sea ice. The oceanic sensible heat flux at ice bottom derives from McPhee (1992).

Since the dynamics and transport of sea ice are not represented in GELATO-1d, biases in e.g. sea ice concentration or thickness may appear in some regions with strong sea ice dynamics. To cope with this issue, sea ice concentration and thickness can be constrained (relaxed or prescribed) with observed or reanalysed data. In this study, only the concentration is prescribed in some experiments.

Sea ice in IFS (ECMWF)

At the start of the APPLICATE project, the ECMWF HRES ten-day deterministic forecasts had fixed ice cover throughout the forecast range. The HTESSEL surface module of the IFS has a 4-layer thermodynamic ice tile with fixed depth (1.5m) which allows the overlying atmosphere to interact with the sea ice surface to solve the surface energy balance over ice covered ocean.

Since June 2018, the HRES forecasts are coupled with the community ocean model NEMO (version 3.4.1) and a dynamic-thermodynamic sea ice model (LIM2) which has been developed at the Belgian Université catholique de Louvain (Fichefet & Maqueda, 1997) and is part of NEMO 3.4.1. The LIM2 sea ice model is relatively simple in that it has a single thickness category including two layers of ice and one of snow, and it does not model some key surface processes, such as the forming of melt ponds. The sea ice model uses a rheological model to describe the internal ice dynamics, and takes rafting and ridging into account. However, at present only the sea ice cover is passed to the IFS model during a so-called “coupling” time step (which is larger than the atmospheric time step). In the following we will refer to this present coupling as to the ‘ice-to-ice’ coupling. Introducing a sea ice model in NWP involves much shorter temporal scales and higher spatial variability compared to those considered in climate models, and special attention is needed for the model initialisation in order to correctly represent the ice-atmosphere coupling. Current data assimilation systems for the atmosphere and ocean are run separately and therefore need to solve their own surface energy balance. Then, IFS computes the surface-atmosphere exchanges and the ice temperature over sea ice using its own thermodynamic model, possibly leading to an inconsistency between the surface temperature in LIM2 and IFS. The impact of a closer thermodynamic coupling between LIM2 and IFS, as well as more details of the coupling methodology used are reported in D2.2.

2.1.2. Snow on land

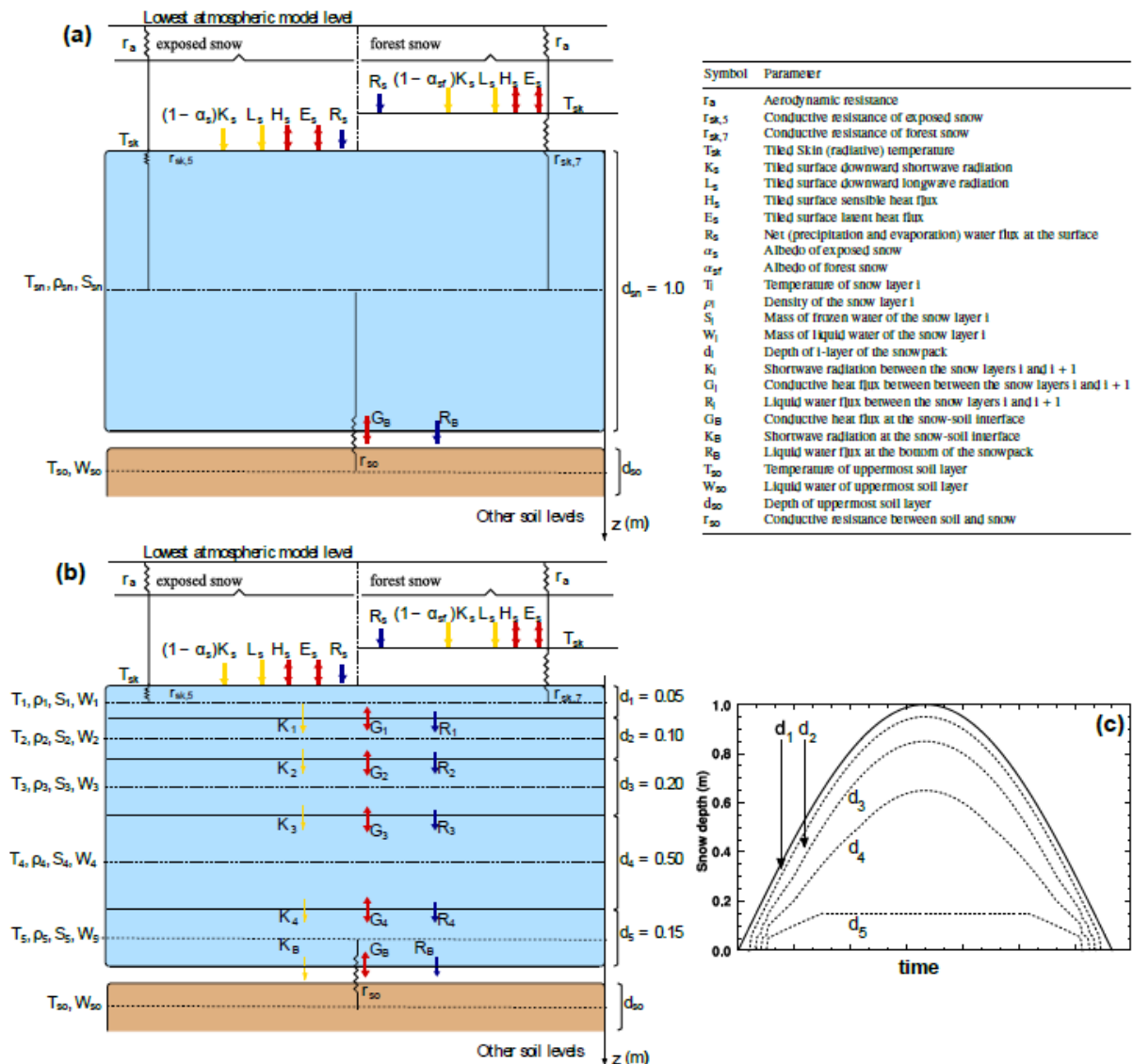


Figure 2.1: Schematics of the (a) single-layer and (b) multi-layer snow schemes; (c) idealized time-series of snow depth accumulation and ablation (continuous line) with the vertical discretization used in the multi-layer scheme (dashed lines). The list of symbols used is also reported.

The multi-layer snow scheme (ML hereafter) introduced in the land-surface model of IFS (HTESSEL, Balsamo et al., 2009) is an intermediate complexity snow scheme following the definition by Boone & Etchevers (2001). It represents the vertical structure and temporal evolution of snow temperature, density and liquid water content and the surface snow albedo. A comparison of the structures of the single-layer (SL) and ML snow schemes and the coupling to the atmosphere and soil is shown in Figure 2.1. ML uses the same parametrizations of snow albedo (both for exposed and forest snow) and snow cover fraction as in SL. A preliminary version of ML implemented in the EC-EARTH climate model was reported by Dutra et al. (2012) and tested in long climate simulations. The main differences between the ML scheme presented and evaluated in this report and the ML implementation of Dutra et al. (2012) concern a set of new snow physics parameterizations, as well as the formulation of the snow vertical layering and of the surface coupling with the atmosphere in case of surface melting. A detailed description of the ML scheme and its initialisation is reported in Arduini et al. (2019).

2.1.3. Snow on sea ice

ECMWF

An option has been added to activate the ML snow scheme from IFS also over sea ice surfaces. Important processes typical of snow over sea ice are missed in ML, like advection or immersion/flooding of sea ice due to snow load. However, the activation of ML over sea ice can inform on:

- the zero-order effects of snow on time scales of a few days, through its impact on surface fluxes (for instance outgoing longwave radiation) and coupling to the ice/ocean underneath.
- the benefits of bringing the thermodynamics of the two models (LIM and IFS) over sea ice closer together.

In the current operational IFS version, HTESSSEL is designed to represent a grid box either as land or ocean, meaning that a mixture of these two main categories is not allowed and snow can only cover a land grid box. With the new modification evaluated within APPLICATE, snow, if present, can also cover the fraction of an ocean grid box that is occupied by ice.

The representation of snow over sea ice surfaces is currently handled differently than the snow on land in ML. The main differences concern the temporal evolution of the snow albedo and roughness throughout the forecast. Indeed, a correct representation of the radiative (albedo) and mechanical (roughness) properties of snow over sea ice would require the parametrization of physical processes which are not considered in the current formulation of the ML scheme, for instance the formation of melt ponds. In the absence of such processes, monthly climatological values of sea ice albedo are used (in the same way as in the current operational system), which are derived taking into account the effect of snow on surface albedo. For the roughness length, the same empirical formulation currently implemented for sea ice is used.

CNRS-GAME

GELATO-1D already includes a single-layer snow model. In GELATO 6, the solar radiative transfer scheme through the snowpack covering sea ice was upgraded following Grenfell and Maykut (1977). The albedo of dry snow, melting snow and melting ice are model parameters, respectively set to 0.88, 0.77 and 0.58.

2.1.4. Arctic atmospheric boundary layer

In cases when it is considered that the cloud type is a stratocumulus layer (i.e., when a cloud is present and the unstable boundary layer is topped by a strong inversion), a cloud-top driven K-diffusion component is added to the surface driven K-diffusion profile. This cloud-top driven K-diffusion is proportional to the cloud-top radiative cooling, following Lock et al. (2000). Previously, the depth of this mixing was assumed to span the whole boundary layer, implying a coupled, well-mixed boundary layer. However, for the Arctic region over sea ice, the boundary layer is more frequently observed to be decoupled during the summer, where turbulent mixing between the cloud and surface is suppressed (e.g. Curry 1986, Sedlar et al. 2012, Brooks et al. 2017). The degree of coupling is important for cloud formation, and in turn, the amount of energy absorbed by the surface. The previous assumption that stratocumulus boundary layers are well-mixed has now been relaxed, and the cloud-top mixing depth is calculated using an air parcel descent. This revision permits an additional BL type, namely decoupled stratocumulus.

SU found that the air parcel updraft in the EDMF scheme often did not diagnose Arctic stratocumulus cloud, thus omitting explicit treatment of cloud-top mixing and entrainment. The scheme has been updated to properly diagnose stratocumulus cloud based on the inversion strength and cloud fraction. In addition, radiatively-driven turbulent mixing in stratocumulus clouds now occurs at the correct height, i.e. below the level at which long-wave cooling is greatest.

2.2. Evaluation of the new components

In this section, we only provide a few elements of the evaluation of the ML snow scheme in IFS. More details can be found in Arduini et al. (2019). For an evaluation of GELATO6 (within the coupled system CNRM-CM6-1), whose 1d version was activated in ARPEGE/AROME, the reader may refer to Voltaire et al. (2019) and references therein.

The evaluation of the ML snow scheme was first performed using the in-situ observations of the Earth System Model Snow Intercomparison Project (ESM-SnowMIP, Krinner et al., 2018; Ménard et al., 2019). This dataset includes meteorological, snow and soil observations from 10 snow reference sites, with at least 7 years of data for each site (some sites having more than 15 years of data). These observations are used to force an offline version of the land-surface model (i.e., uncoupled from the atmospheric model). This enables the evaluation of the ML snow scheme at the process-level, as the uncertainties arising from misrepresented atmospheric perturbations are removed. Two configurations of the ML snow scheme are evaluated at the ESM-SnowMIP sites and compared to a control experiment using the current SL snow scheme:

- a configuration named ML-Std, which uses a maximum number of snow layers $N_{max} = 5$. The snow physical parameterizations are the same as the ones used for SL;
- a configuration named ML-Opt, in which a new set of physical parameterizations are added to the ML-Std: new snow heat conductivity, solar absorption by the snowpack, wind-induced compaction and modified basal heat resistance. See Appendix A of Arduini et al. (2019) for details on the parameterizations.

Normalised Root-Mean-Square-Error (NRMSE) statistics for snow water equivalent (SWE) and snow depth (SD) for two different seasons – December-January-February (DJF), and March-April-May (MAM) – are shown in Figure 2.2. For SWE and SD, all the sites with sufficient data to perform the evaluation were selected (6 and 8 out of 10 sites respectively). The RMSE is normalised by the standard deviation of observations for each site, so that performances at different sites can be quantitatively compared. Due to the small number of observations of SWE at the available BERMS sites (obs, ojp), these sites have been excluded from the computation of the NRMSE for SWE.

Overall, ML-Std and ML-Opt show a general improvement in simulating SWE and snow depth compared to SL. The main improvements are in snow depth, for which the total NRMSE averaged over all sites is reduced by more than 30% for both ML experiments. The improvements in the simulation of SWE are not as large, showing a seasonal dependency and some deterioration at the most complex mountainous sites. The total NRMSE of SWE averaged over all sites during DJF is reduced by approximately 9% in ML-Opt and ML-Std compared to SL. During MAM, it is reduced by 12.5% and 6.8% for ML-Opt and ML-Std, respectively, demonstrating the importance of the added processes in ML-Opt to improve the representation of the energy balance of the snowpack.

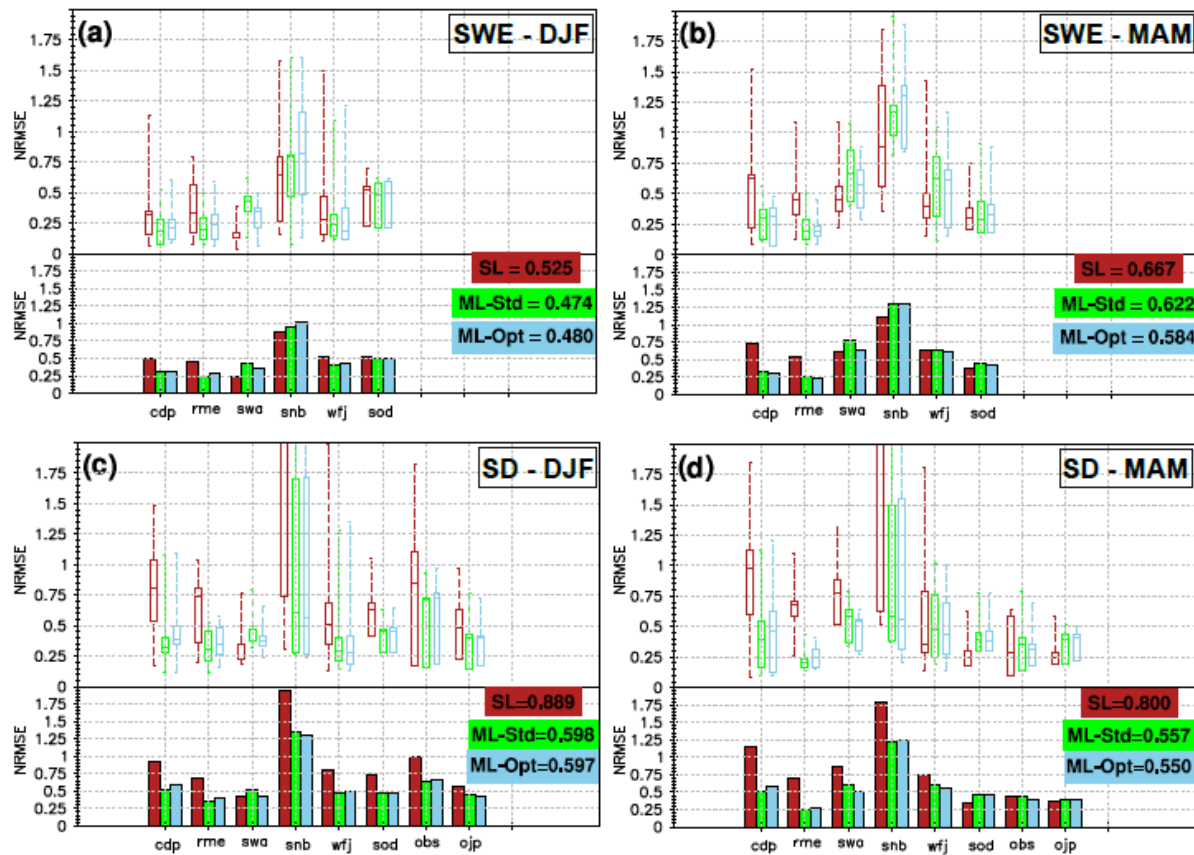


Figure 2.2: Top row: summary statistics of normalized root-mean-square-error (NRMSE) of snow water equivalent (SWE) at each site for (a) DJF and (b) MAM for the offline experiments using the single-layer (SL, red), multi-layer standard (ML-Std, green) and multi-layer optimized snow scheme (ML-Opt, blue); Top panel: boxplot of the distribution of yearly NRMSE; boxes have horizontal lines at the lower, median and upper quartile and the vertical dashed lines extend from the minimum to maximum value. Bottom panel: total (computed for all years) NRMSE at each site; the numbers in the boxes show the mean (for all sites) value of NRMSE for each experiment. Bottom row: same as the top row, but for the snow depth (SD).

Figure 2.3 shows time-series at two selected sites for three seasons, to highlight the differences between SL and ML. Col de Porte is an Alpine site characterized by moderately mild winters in which liquid precipitation and melting events can occur anytime during the snow season (Morin et al., 2012). Sodankylä is an Arctic site, characterized by lower snowfall amount, lower temperatures during wintertime and fewer melting episodes during the snow season, compared to Col de Porte. At Col de Porte, the temporal evolution of SWE is largely improved throughout the season, which results in an improved representation of the timing of the final ablation. This can be associated to the lower thermal inertia of the top (thin) snow layer, which makes ML more responsive to sporadic melting and refreezing events than SL.

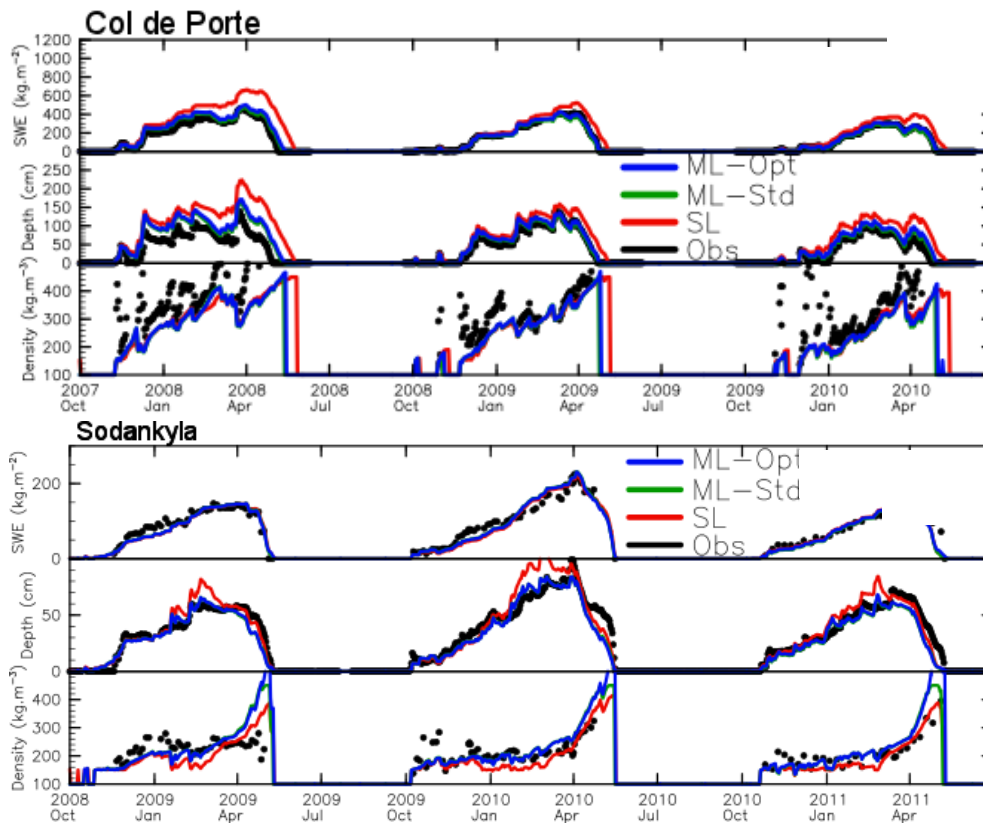


Figure 2.3: Time-series of snow water equivalent (SWE), snow depth and snow density for (a) Col de Porte and (b) Sodankylä from observations and the offline experiments using the single-layer (SL, red lines), multi-layer standard (ML-Std, green lines) and multi-layer optimized snow scheme (ML-Opt, blue lines).

At Sodankylä, there are small differences of SWE between SL and ML. For the snow depth, there is a positive and negative impact during the accumulation (DJF) and melting (MAM) periods, respectively (see Figure 2.3). The improvement during the accumulation period is explained by a better representation of snow density during this period. On the other hand, the snow density increases too quickly during the final ablation phase, explaining the degradation of the snow depth statistics during MAM.

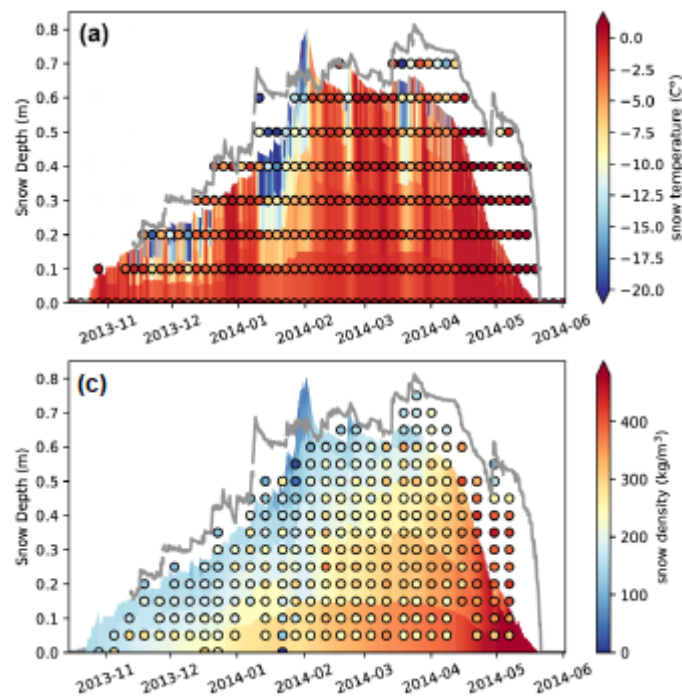


Figure 2.4: Time-depth plot of snow temperature (a) and density (b) at Sodankylä from the offline simulations using the multi-layer snow scheme (ML-Opt, background colours) and observations (coloured dots) for the 2013/2014 season. Snow depth from observations is superimposed (grey line).

Figure 2.4 shows time-height plots of snow temperature and density at Sodankylä, from observations and from the offline ML-Opt experiment. Snow temperature is measured by an array of thermistors that is covered by snow during wintertime, while snow density profiles are measured every week or so by digging a pit in the snow and weighing a snow sample of a certain volume (Leppänen et al., 2016; Essery et al., 2016).

The multi-layer snow model captures the propagation of heat/cold waves within the snowpack (see Figure 2.4a), a key feature of Arctic environments during wintertime (Miller et al., 2017; Persson et al., 2017). A qualitative comparison of the modelled temperature with observations at the same depth from the top snow surface suggests that the downward propagation of this cold wave through the snowpack is well represented by the model. The temporal evolution of snow density also looks realistic throughout the season (see Figure 2.4b), even though the snow density of the bottom of the snowpack is overestimated by the model, particularly after February 2014. This could be due to the relatively simple parameterization of metamorphism implemented in ML, which does not allow complex snow crystal evolution to be represented (e.g. depth hoar formation).

To evaluate to what extent the results at specific sites are valid at a broader spatial scale, global uncoupled simulations (offline) were run with the land-surface model using the single-layer (SL) and multi-layer snow scheme (ML-Opt). The simulations are forced using the ERA5 meteorological reanalyses dataset and cover the time period 2010-2018. Simulated snow depth is compared to observations from the global SYNOP network for the time period 2014-07-01 to 2018-05-31.

Figure 2.5 shows the difference in RMSE of snow depth between ML-Opt and SL for the December to May (DJFMAM) period. Summary statistics averaged over all available stations are reported in the plot. ML-Opt improves the simulation of snow depth, reducing the RMSE by about 12% compared to SL, which generalizes the results obtained for the local sites to the global scale. The improvements are mainly due to an improved representation of snow density and of sporadic melting events (see Arduini et al., 2019). The only region showing a small detrimental impact is the eastern part of the Scandinavian peninsula. This can be partially due to an overestimation of snow density compaction in this region during the melting season (as shown for Sodankylä, cf. Figure 2.3b), as well as in the forcing fields like the solid precipitation, which is weakly constrained in the reanalysis. The analysis of time-series averaged over the SYNOP stations in the northern hemisphere show that SL generally overestimates

the increase of the snow depth during the accumulation period. The ML experiments simulate better the temporal evolution of snow depth compared to the observed one, therefore improving both accumulation and ablation periods (see Figure 2.6). The differences between ML-Std and ML-Opt are small at the global scale, with a slightly better performance of ML-Opt during the ablation season.

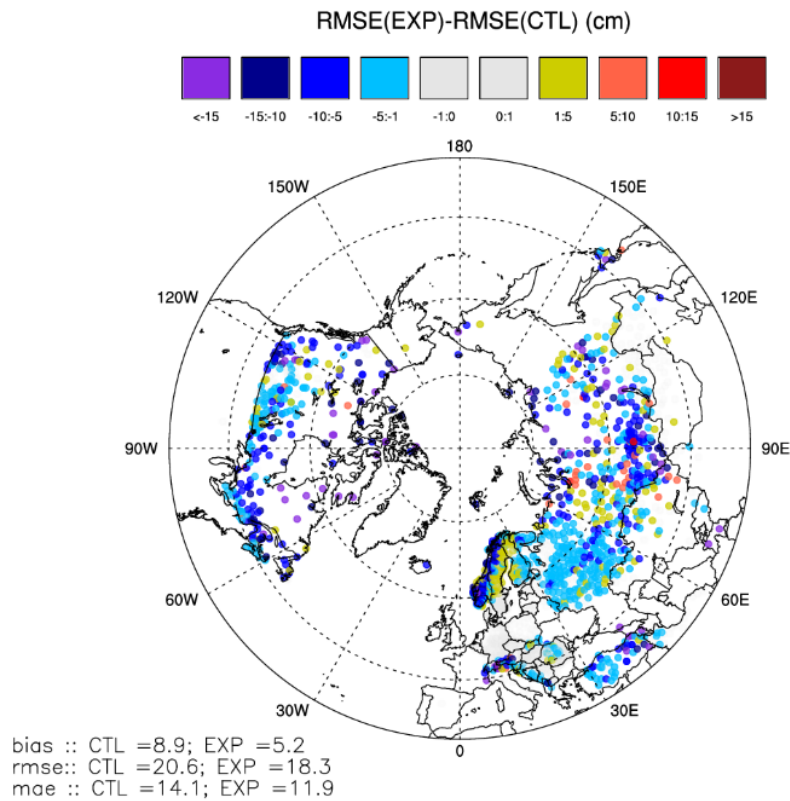


Figure 2.5: Difference in root-mean-square error (RMSE) of snow depth (cm) between the global offline experiment using the multi-layer (ML-Opt, EXP) and single-layer (SL, CTL) snow schemes from December to May (DJFMAM) between 2014 and 2018.

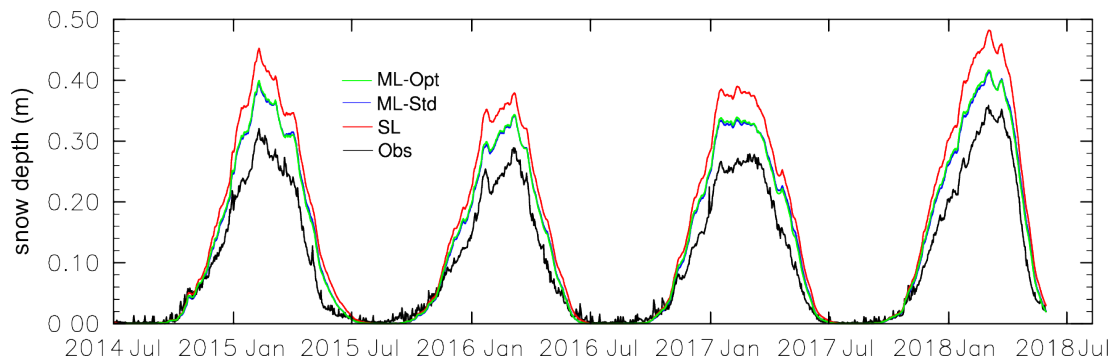


Figure 2.6: Time series of snow depth averaged over all SYNOP stations available in the Northern Hemisphere over the time period 2014-07-01 to 2018-05-31 from observations (Obs, Black line), SL (red line), ML-Std (blue line) and ML-Opt (green line).

2.3. Experimental protocol

2.3.1. Implementation of GELATO-1D into AROME and ARPEGE (CNRS-GAME)

Regional coupled AROME/SURFEX and ARPEGE/SURFEX forecasts were performed over the Arctic and global domain respectively. The AROME/SURFEX model was used in a dynamical adaptation from the global model ARPEGE/SURFEX (no assimilation cycle). GELATO-1d sea ice model uses a sea ice fraction (FSI), this fraction can be derived from the sea surface temperature (SST) analysis based on the OSTIA product (Donlon et al., 2012) following two strategies:

- **B** ('binary sea ice fraction'). Only SST data is used. To reduce the spin-up, a first AROME-GELATO-1D 24h-forecast is run one day before the start of the study period coupled with the global operational numerical weather prediction model ARPEGE. In this first forecast, FSI is defined to 1 if the SST is below the freezing point and 0 elsewhere. Denoting T_f the seawater freezing point, SST_0 the SST used for the forecast initialisation and FSI_{24h} (the 24h sea ice forecast), FSI is defined as follows for each of the subsequent forecast:

- If $SST_0 \leq T_f$ and $FSI_{24h} > 0$, $FSI = FSI_{24h}$
- If $SST_0 > T_f$ and $FSI_{24h} > 0$, $FSI = 0$
- If $SST_0 \leq T_f$ and $FSI_{24h} = 0$, $FSI = 1$

- **F** ('OSI-SAF sea ice fraction'). Here, in addition to the SST analysis, the OSI-SAF sea ice fraction is used and denoted as FSI_0 . For the first 24h forecast, $FSI=FSI_0$ then, it is defined as follows:

- If $FSI_0 > 0.05$, $FSI = FSI_0$
- If $FSI_0 \leq 0.05$ and $SST_0 \leq T_f$, $FSI=0.05$
- If $FSI_0 \leq 0.05$ and $SST_0 > T_f$, $FSI=0$

Finally, where there is sea ice ($FSI > 0$), SST is set to T_f , and $SST=SST_0$ elsewhere.

The initial values of the main prognostic variables are given in Table 2.1. Several tests have shown that they must be initialized in a consistent way (e.g. surface temperature and vertical temperature profile in sea ice) to avoid spin-up issues.

GELATO variable	Description and unit	Initial value
FSI	Sea ice fraction (0-1)	Computed from OSTIA SST and/or OSI-SAF sea ice concentration data
HSI	Sea ice thickness (m)	1
HSN	Snow thickness (m)	0
SSI	Sea ice salinity ($g.kg^{-1}$)	5
TSF	Sea ice (or snow) surface temperature ($^{\circ}C$)	-15
T_i	Sea ice and snow layers temperature ($^{\circ}C$)	Linear vertical profile from seawater freezing point (bottom) to TSF (top)
H_i	Sea ice and snow layers enthalpy ($J.m^{-3}$)	Calculated as a function of T_i and SSI

Table 2.1: Definition of the main prognostic variables of GELATO-1D and their initial values. T_i and H_i are vertical profiles, where the i index ranges from 1 to 9 for the sea ice part of the slab, and $i=10$ for the overlying snow layer.

The choice of setting the initial sea ice temperature to a spatially uniform $-15^{\circ}C$ may seem to be a crude one, but surface temperature quickly adjusts to the atmospheric conditions during the forecast. Finally, to evaluate the impact of the coupling of the sea ice model, four experiments have been performed:

- **ArpAro-R**: is the reference experiment with ARPEGE AROME without GELATO-1d

- **ArpAroG-B:** ARPEGE AROME-GELATO ‘Binary’; GELATO-1d is only activated within AROME-SURFEX, and the sea ice fraction data used as initial condition is calculated following the ‘binary case’ (from OSTIA SST data)
 - **ArpAroG-F:** ARPEGE AROME-GELATO ‘Fraction’; same as **ArpAroG-B** but with a sea ice fraction between 0 and 1 deduced from the OSI-SAF sea ice fraction and the SST analysis
 - **ArpGAroG-F:** ARPEGE-GELATO-AROME-GELATO ‘Fraction’; GELATO-1d is activated both within ARPEGE-SURFEX and AROME-SURFEX, and the sea ice fraction data is initialized from the OSI-SAF sea ice fraction and the SST analysis in ARPEGE-GELATO. This experiment was designed to improve the accuracy between the surface variables and the boundary layer in the initial conditions used by AROME-GELATO computed from the ARPEGE-GELATO.
- The configurations of the 4 experiments are detailed in Table 2.2.

	ArpAro-R	ArpAroG-B	ArpAroG-F	ArpGAroG-F
Model	Dedicated APPLICATE/YOPP version of Météo-France AROME			
Model version	Cy43_op1			
Upper air assimilation/initialization	Dynamical adaptation from the operational global Arpege production model. The cut-off time is 2h15 min for the 0000UTC analysis			
Surface assimilation/initialization	Dynamical adaptation from the operational global Arpege production model	Dynamical adaptation from the operational global Arpege production model. GELATO variables copied from day-1		Dynamical adaptation from the operational global Arpege-GELATO production model
Model runs per day	0000UTC +48h			
Resolution	2.5 km, 65 L (~ 14 levels below 500m)			
Sea ice and sea surface temperature	Sea ice and SST prescribed from OSTIA (constant during integration)		SST prescribed from OSTIA (constant during integration). Sea ice fraction assimilated from OSISAF.	SST prescribed from OSTIA (constant during integration). Sea ice fraction assimilated from OSISAF (calculated in Arpege).
Surface model and snow treatment	SURFEX with 1-layer snow scheme; prognostic water equivalent, snow density and surface albedo. Soil scheme ISBA	SURFEX-GELATO with 1-layer snow scheme; prognostic water equivalent, snow density and surface albedo. Soil scheme ISBA		
Boundary conditions	ARPEGE from same cycle (hourly coupling)	LBC; ARPEGE from same cycle (hourly coupling).		LBC; ARPEGE-GELATO from same cycle (hourly coupling)

Table 2.2: Configurations used for the ARPEGE/AROME experiments to test the impact of including GELATO-1d

2.3.2. Implementation of LIM2 into IFS (ECMWF)

On 5 June 2018, the LIM2 sea ice model was implemented in IFS Cycle 45r1. For this deliverable, we compare the impact of using LIM2 (dynamic sea ice model) with the previous framework which keeps sea ice cover fixed for the duration of the forecast. We present a 10-day forecast case study (1st April 2018) using a coupled ocean-atmosphere model at a horizontal resolution of about 9km for the atmosphere and 25km ocean model. In the configuration without interactive sea ice, the sea ice concentration is fixed to the OCEAN5 reanalysis for the duration of the forecast.

2.3.3. Snow on land (ECMWF)

Global land-atmosphere forecasts were performed using the IFS Cycle 45r1 with the single-layer (FC-SL) and multi-layer (FC-ML) snow schemes for December 2016 to March 2017, using a horizontal resolution of 30 km and 137 vertical levels, with the lowest model level being located at about 10 m above the ground. The atmospheric fields are initialized using the ECMWF operational analysis. The surface fields of the FC-SL and FC-ML forecasts are initialized from global uncoupled (offline) simulations using the SL and ML schemes. These offline simulations cover the time period from June 2010 to June 2018 and were forced with reanalysis atmospheric data.

2.3.4. Snow on ice (ECMWF)

Coupled forecasts were performed from 1st January to 21st January 1998, using a horizontal resolution of 9 km and 137 vertical levels, with the lowest model level being located at about 10 m above the ground. This is the configuration currently used in operational HRES ten-day forecasts at ECMWF. Forecasts are initialised every day at 00UTC from the ECMWF operational analysis. Two experiments are designed and compared:

- a simulation with no representation of snow over sea ice, used as control (*ctl*);
- a simulation in which the ML snow scheme is active also over sea ice surfaces (*snow*).

2.3.5. Atmospheric boundary layer (SU)

The IFS single column model (SCM), Cycle 43r3 was run for a 5-day period from the ASCOS 2008 field campaign in the Arctic Ocean. The model was run for multiple 24-hour periods from 26-30 August 2008 using initial and boundary conditions from the ERA5 re-analysis data, for a total of 10 simulations. These simulations used 137 vertical levels, with the lowest level at 11.5 m above the surface. Two experiments are compared:

- a control experiment using the original boundary layer scheme (denoted CTL);
- an experiment using the revised boundary layer scheme (denoted NEW).

3. RESULTS AND DISCUSSION

3.1 Impact of an interactive sea ice scheme on ARPEGE/AROME forecasts

The impact of the GELATO-1d interactive sea ice scheme on AROME forecasts is evaluated using instantaneous 2m air temperature observations from the Norwegian Meteorological Institute (eklima.met.no, Figure 3.1). They were flagged as ‘high quality observations’ and are described in Kølitzow et al. (2019).

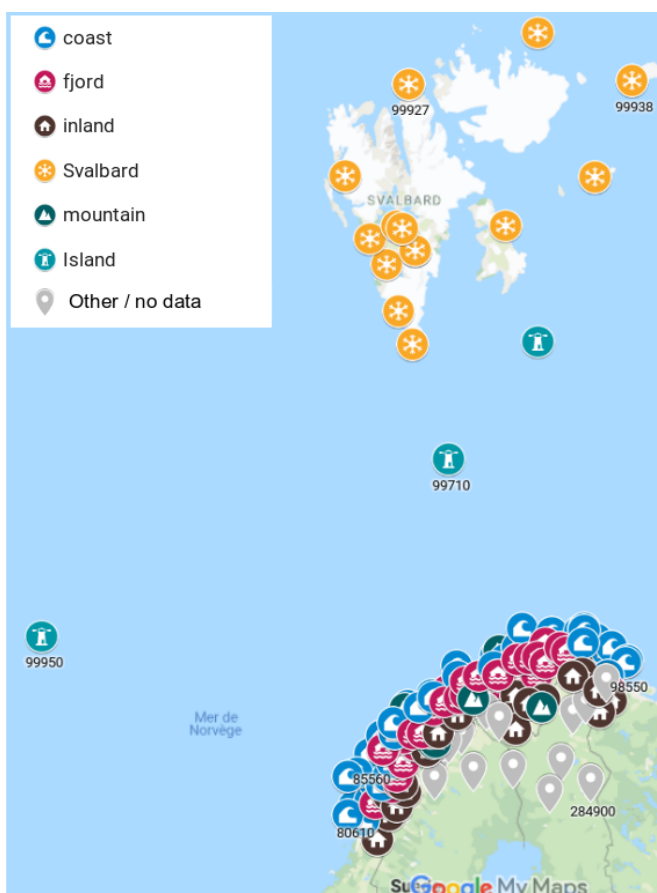


Figure 3.1: Location of the APPLICATE observation stations. Source: https://drive.google.com/open?id=1a9w7Z-ivUa0HfXNfhsmo_j-eA9Y4XZW6&usp=sharing

These observations sites have been classified into six regions: Svalbard (14 stations), islands (3 stations), coast (40 stations), fjords (39 stations), inland (25 stations) and mountains (9 stations). The assignment of each station to a region is done subjectively by operational forecasters at MET Norway based on their knowledge about individual stations (Kølitzow et al, 2019). The Kvitøya Station (number 99938, in Svalbard, see Figure 3.1) was chosen to compare the forecast T_{2M} of different experiments with observations (Figure 3.2). We chose this weather station because it is the closest to the ice edge, where T_{2M} can be very sensitive to the experimental set-up.

We present hereafter the results of the three experiments:

- **ArpAroG-B experiment** (binary sea ice fraction)

The activation of GELATO-1d with a binary initialization from OSTIA allows for an improved behaviour of the simulated T_{2m} until 1st March (Fig 3.2a). This already present in the reference experiment (Arp-Aro-R) that uses a climatological sea ice temperature. However, large underestimations can be seen at grid-cell level as in Figure 3.2.b (e.g. period 3-10 March). This is due to an overall overestimation of the initial sea ice fraction derived from the SST analysis since a partial sea ice coverage of individual grid-

cells is not an option. This overestimation leads to too cold surface temperatures on the sea ice edge where the temperature should be close to the seawater freezing point over the ocean in a fraction of the grid cells. The next experiment attempts to correct this limitation of the initial experimental protocol.

• **ArpAroG-F experiment (sea ice product)**

The use of a sea ice fraction product to initialize the model allows to reduce drastically the mean T_{2M} bias with respect to observations (by up to 7°C), especially during periods with strong temperature variations such as 3-7 or 22-28 February. However, one can notice sudden T_{2M} drops to values close to those from the ArpAro-R experience (e.g. 22-28 February). This behaviour is explained by the atmospheric initial conditions derived from the ARPEGE model which is not coupled to GELATO-1d.

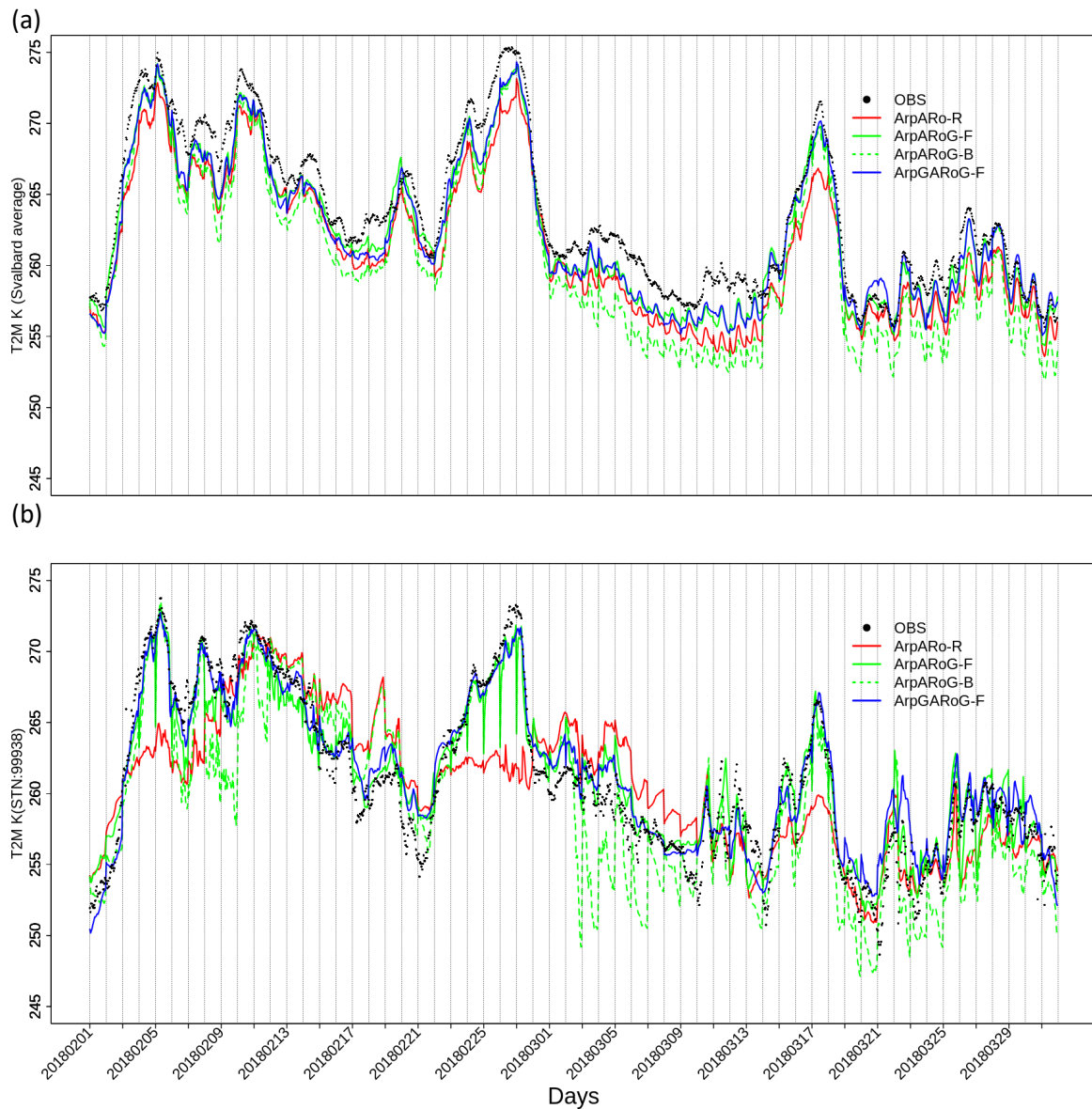


Figure 3.2: (a) Mean of T_{2M} for all Svalbard stations and (b) T_{2M} for station number 99938 on Svalbard for SOP1 period and for ArpAro-R, ArpAroG-F, ArpAroG-B and ArpGARoG-F experiments.

• **ArpGAroG-F experiment**

The last experiment is the same as the previous one ArgAroG-F, except that it benefits from initial conditions from ARPEGE coupled with GELATO-1d. The atmospheric initial conditions are balanced with the surface initial conditions, explaining the smoother T_{2M} forecast (Figure 3.2.b). This configuration is the one that produced the best results and the rest of this section provides more details of its evaluation.

The activation of the GELATO-1d sea ice model in the SURFEX surface platform included in ARPEGE/AROME also substantially improves the forecast 2m temperature (T_{2M}) for the entire SOP1 period. Figure 3.3 shows the average bias and standard deviation errors for the different regions considered for this experiment and the reference (ArpAro-R). The impact of interactive sea ice on the forecasts over remote regions with respect to the sea ice edge, e.g. mountain and inland stations from mainland Norway is relatively weak (Figure 3.3. top). By contrast, there is a clear positive impact on the Svalbard region and for all the selected stations (Figure 3.3. bottom). However, the positive impact for the fjord region is unexpected. Several hypotheses such as discrepancies between SST analysis, OSISAF sea ice fraction product and land-sea mask are still under investigation to explain this improvement. The improvement of T_{2M} forecasts over fjord stations should yet not be regarded as an added-value of the interactive sea ice model. The average bias and standard deviation errors over the Svalbard stations where sea ice was present during the period (Figure 3.4.a) are strongly reduced (Figure 3.3.a). A strong improvement of T_{2M} forecasts is seen over every single station of the Svalbard region as shown on Figure 3.3.b, even though the amplitude of the impact varies with the chosen station.

Figure 3.4.b-c illustrates the impact of coupling the GELATO-1d sea ice model with AROME on spatial maps of forecast T_{2M} . The temperature gradient is smoother at the sea ice edge with the use of the sea ice model. The lower atmosphere tends to be warmer on average. This is particularly true in the north-east of the Svalbard region and the model turns out to be in better agreement with observations (Figure 3.4.c).

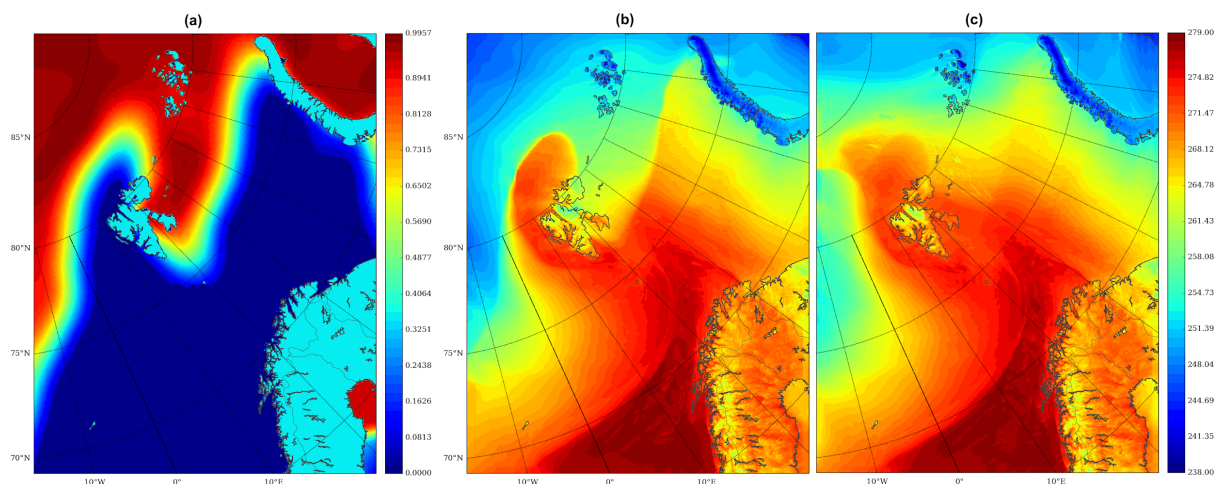


Figure 3.3: Sea ice fraction derived from observations used to initialize the forecast (a), March 17 at 00 UTC. Two-meter temperature over the whole domain without (b) and with the use of the GELATO-1d sea ice model (c) within the SURFEX platform.

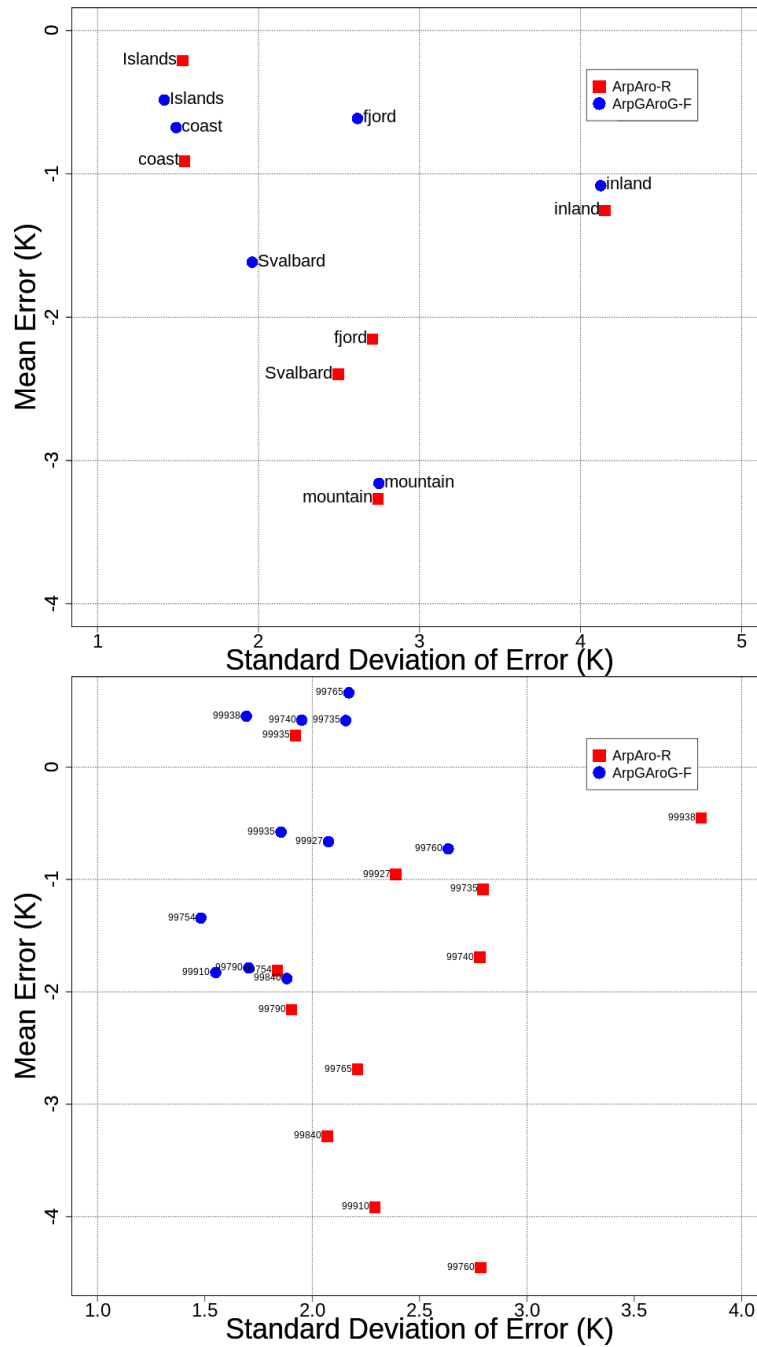


Figure 3.4: Mean error versus SDE of the 24h forecasts for two-meter temperature during YOPP SOP-NH1 period. The forecasts are initialized at 00 UTC. Average per region (top), all the Svalbard stations (bottom).

3.2 Impact of interactive sea ice on IFS forecasts

The case study presented here illustrates the impact of including the LIM2 sea ice model in HRES forecasts. Forecasts including or not an interactive sea ice are compared over the Baltic Sea and evaluated using the analysis of sea ice concentration from the OCEAN5 reanalysis. Other case studies illustrating the impact of a dynamic sea ice on forecasts and the evaluation of the impact in the Northern Hemisphere for different seasons are described in detail in Keeley and Mogensen (2018).

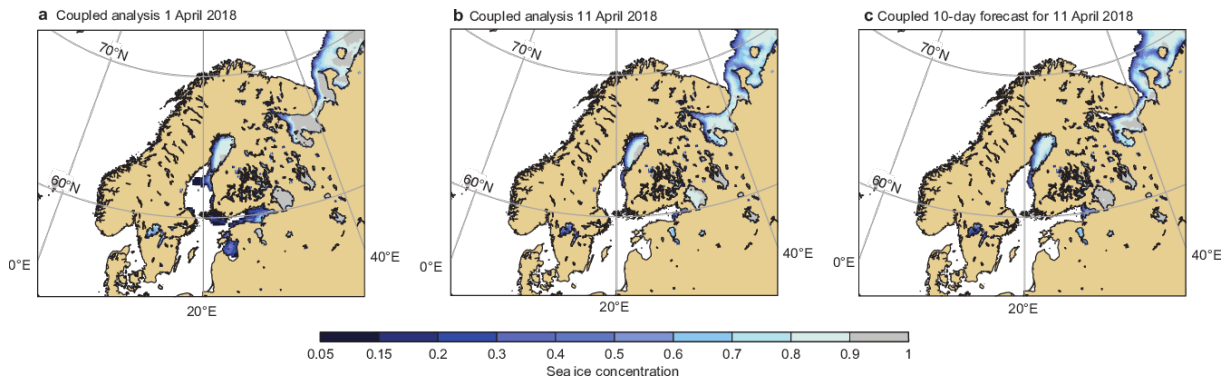


Figure 3.5: Performance of HRES sea ice concentration predictions with dynamic sea ice. The plots show (a) the HRES coupled analysis of sea ice concentration based on OCEAN5 for 1 April 2018, (b) the HRES coupled analysis for 11 April 2018 and (c) the HRES coupled 10-day forecast for 11 April 2018.

Figure 3.5 illustrates the impact of having a coupled sea ice model within the HRES forecasts. Figure 3.5b shows the state of the ice in the OCEAN5 analysis for 11 April 2018. Compared to the OCEAN5 analysis for 1 April shown in Figure 3.5a, over the course of ten days, the ice has retreated within the Gulfs of Finland, Riga and Bothnia. Sea ice concentration can have a strong impact on predictions of local 2-metre temperature, although the size of the impact depends on how the surface fluxes are altered by local meteorological conditions (e.g. the overlying atmospheric temperature) and the concentration; where concentrations are high, the heat flux from the ocean to the atmosphere is significantly reduced. To illustrate this, Figure 3.6 shows the difference in sea ice concentration and temperature between 24-hour high-resolution forecasts with and without ocean–sea ice–atmosphere coupling. The differences in predicted temperature (Figure 3.6.b) in the Gulf of Bothnia of up to 6°C can largely be attributed to the differences in sea ice concentration (Figure 3.6.a). The size of the changes in 2-metre temperature also depends on the large-scale meteorology.

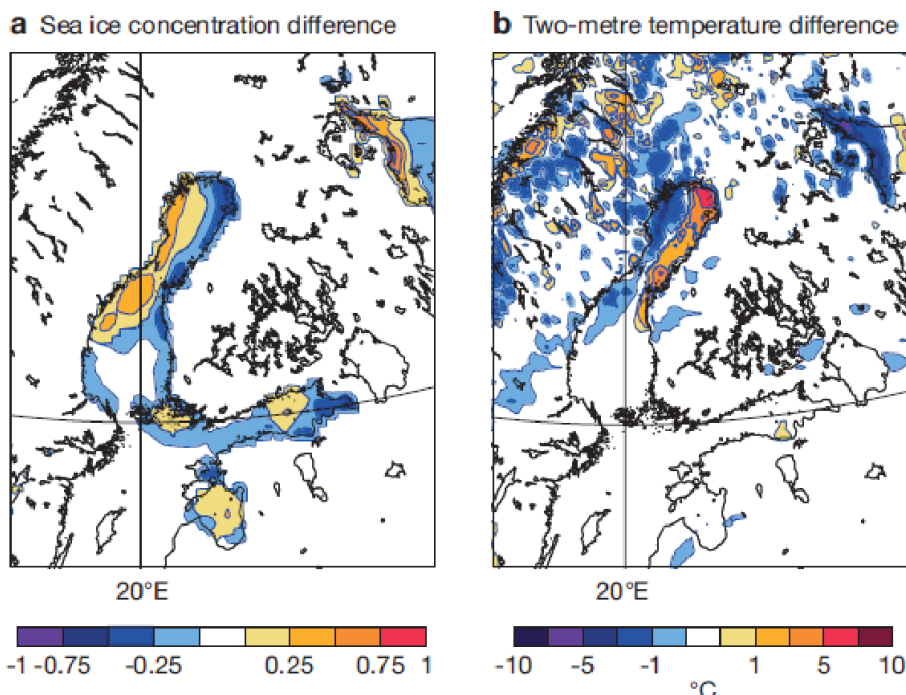


Figure 3.6: Difference between uncoupled and coupled 24-hour HRES forecasts for 2 April 2018 00 UTC (uncoupled minus coupled) for (a) sea ice concentration and (b) 2-metre temperature.

3.3. Impact of snowpack enhancements on IFS forecasts

The analysis focuses on a single reference site using 2m temperature (T2m) and cloud cover observations from the Sodankylä observational supersite, to demonstrate the impact of the multi-layer snow scheme on near-surface weather forecasts over land. It focuses on day 2 forecasts, as it is easier to disentangle the errors associated to the snow-atmosphere coupling from the ones due to cloud forcing at a short lead time. A more extensive evaluation of the impact on 2-metre temperature (T2m) in coupled forecasts is reported in D2.5, D5.3 and Arduini et al. (2019).

The wintertime variability of T2m at the Sodankylä site is mainly driven by cloud cover variations (Figure 3.7), which significantly impact the surface energy balance at high latitudes, by controlling the downward longwave radiative fluxes (Betts et al., 2014; Persson et al., 2017). Extremely low minimum temperatures ($T2m < -20\text{ }^{\circ}\text{C}$) are associated with clear-sky conditions in the observations (Figure 3.7). FC-ML generally improves the simulated T2m for cold episodes, even though the forecast performance depends on the simulated cloud cover (see Figure 3.7).

FC-SL underestimates the amplitude of the diurnal cycle in March by $3.8\text{ }^{\circ}\text{C}$ (Figure 3.8a), with warmer minimum and colder daytime maximum temperature. FC-ML improves the representation of the minimum temperature by almost $1\text{ }^{\circ}\text{C}$, thus reducing the amplitude bias to $2.7\text{ }^{\circ}\text{C}$. The improvement of the diurnal cycle in FC-ML is larger if cloud-free conditions only are selected, although this reduces the number of days over which the statistics are computed (see Figure 3.8a and 3.8b). For such cases, the overestimation of the night-time temperature for FC-SL is an average of about $3.9\text{ }^{\circ}\text{C}$, whereas for FC-ML it is of only $1.8\text{ }^{\circ}\text{C}$.

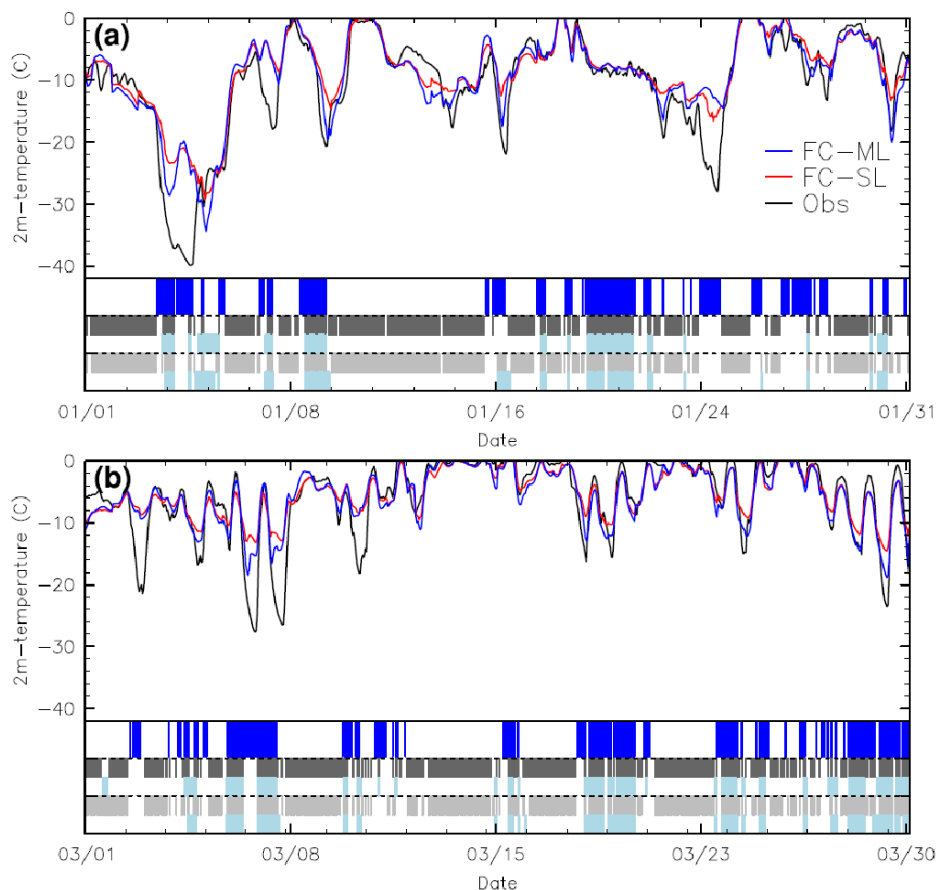


Figure 3.7: Concatenated day 2 ($t+24$ to $t+47$) forecasts of 2-metre temperature ($^{\circ}\text{C}$, top panel) at Sodankylä (Finland) for (a) December 2016 and (b) March from the coupled forecast experiments using single-layer (FC-SL, red line) and multi-layer (FC-ML, blue line) snow schemes, compared to observations (Obs, black line); in the bottom panels, blue squares identify periods of clear-sky in Obs (total cloud cover less than 0.20); the grey squares in each panel identify periods when there is agreement between observed and simulated cloud cover for FC-SL (light grey) or for FC-ML (dark grey); the light blue squares identify periods of clear-sky in the simulations.

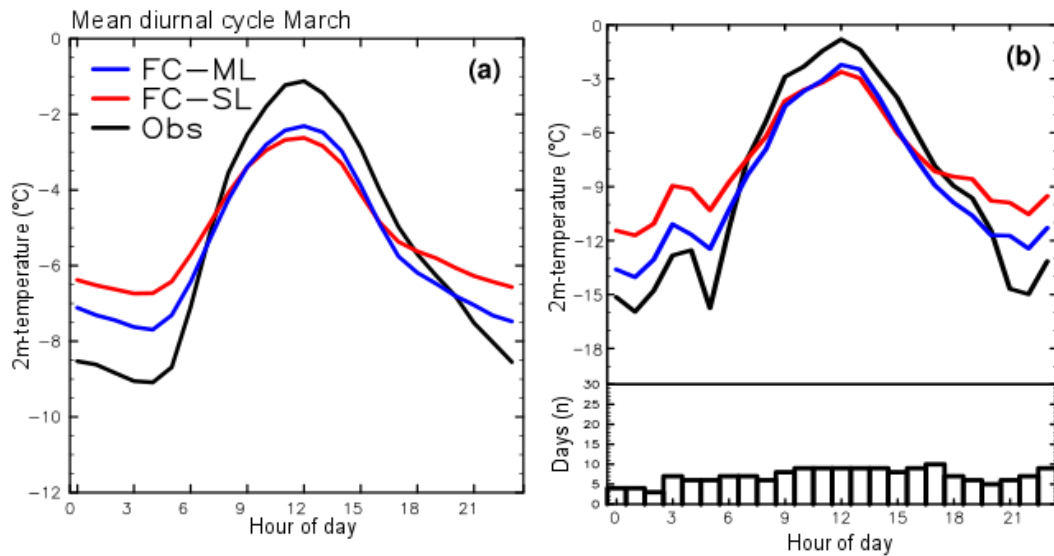


Figure 3.8: mean diurnal cycle of 2-metre temperature at Sodankylä for March 2017 for observations (black line), and the coupled forecast experiments in day 2 ($t+24$ to $t+47$) using the single-layer (FC-SL, red line) and the multi-layer snow scheme (FC-ML, blue line); (b) same as (a) but only for periods of clear-skies both in the observations and in the forecasts. In (b), the histogram displays the number of cases (in days) used to compute the mean diurnal cycle, based on the clear-sky agreement between the observations and the forecasts for each hour-of-day.

3.4. Impact of snow on ice on IFS forecasts

The analysis on the impact of the snow over sea ice uses composited observations from the SHEBA campaign (Persson et al., 2017). We compare a simulation with no representation of snow over sea ice (*ctl*) to a simulation in which the ML snow scheme is active also over sea ice surfaces (*snow*), both covering 1st January to 21st January 1998.

During the considered time period, snow was observed over the sea ice with a relatively constant depth of 24 cm (see Figure 3.9). The *snow* experiment shows an underestimation of snow depth of about 8 cm.

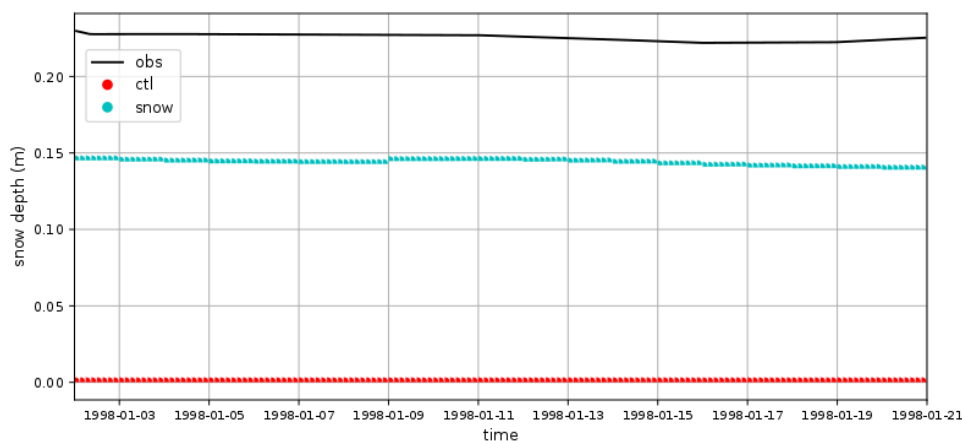


Figure 3.9: time series of snow depth from SHEBA observations (black line) and concatenated forecasts ($t+24$ to $t+47$) at day 2 for the control (red dots) and snow (cyan dots) experiments.

Similarly, for the snow on land at Sodankylä, the wintertime variability of skin temperature is mainly driven by cloud cover variations at this site (see Figure 3.10). For the SHEBA case, the simulated total liquid and ice water path can also be evaluated with observations. Low values of these quantities can be used to identify periods of a weaker impact of clouds longwave radiative flux to the surface energy budget. It should be noted that a model using a prognostic cloud scheme can simulate a cloud cover of 100% even though the liquid and ice cloud water content are small.

A striking feature of the analysed case study is the interplay between errors in the cloud phases and the temporal evolution of the skin temperature. **snow** largely outperforms **ctl** in the simulation of skin temperature, with a good correspondence to the observed skin temperature variability. The improvement is mainly due to the reduction in the **snow** experiment of the heat flux from the ice underneath, compared to that in **ctl**, which enables the surface to radiatively cool (3.11a and 3.11b). An estimation of the heat flux into the snowpack can be obtained from observations as the residual of the sum of the other fluxes, assuming the surface balance to be closed. However, this is not often the case as errors in the calculation of the other terms can be comparable in magnitude to the heat flux into the snow making it difficult to quantitatively evaluate this term.

Often during periods characterised by small values of liquid and ice content, the **snow** experiment simulates a 100% cloud cover (see Figure 3.10). This can happen in the case that the atmospheric temperature decreases as a response to the surface cooling and so leading to a rapid increase of relative humidity in the lowest part of the atmosphere. Despite this, the difference in the downwelling longwave radiative heat flux is less than 5% in the two experiments for most of the analysed period (see Figure 3.11c), therefore implying that the difference in cloud cover has a marginal effect on the longwave radiative forcing at the surface.

However, in cloudy conditions the picture is more complex. For most of the analysed time period, the model shows a large underestimation of liquid water clouds, which largely control the variability of downwelling longwave radiative flux (cf. red lines and symbols in Figure 3.11a and 3.11b). In these periods, the response of the skin temperature to the wrong atmospheric forcing is weaker in **ctl** than in **snow**, therefore the former showing smaller errors compared to observations than the latter (see for instance between 1998-01-03 to 1998-01-05). Overall, the RMSE of skin temperature in day 2 is 4.68°C for **ctl** whereas it increases to 5.23°C for the **snow** experiment (see also Table 3.1). The changes of RMSE are mainly due to a dramatic change of the bias, mainly associated with periods when there are errors in clouds (**ctl** has a positive bias of 1.33°C, whereas for **snow** the bias is of -3.1°C). This points to the key role of compensating errors in the surface energy balance, and the need to address systematic biases of cloud water phase in the Arctic boundary layer during wintertime. The increased surface cooling in **snow** also decreases the temperature at 10m (T10m), which is the height of the first model level, because of the turbulent sensible heat flux. The impact of snow on T10m is overall positive, decreasing the bias and RMSE but slightly increasing the standard deviation of the error (see Table 3.1).

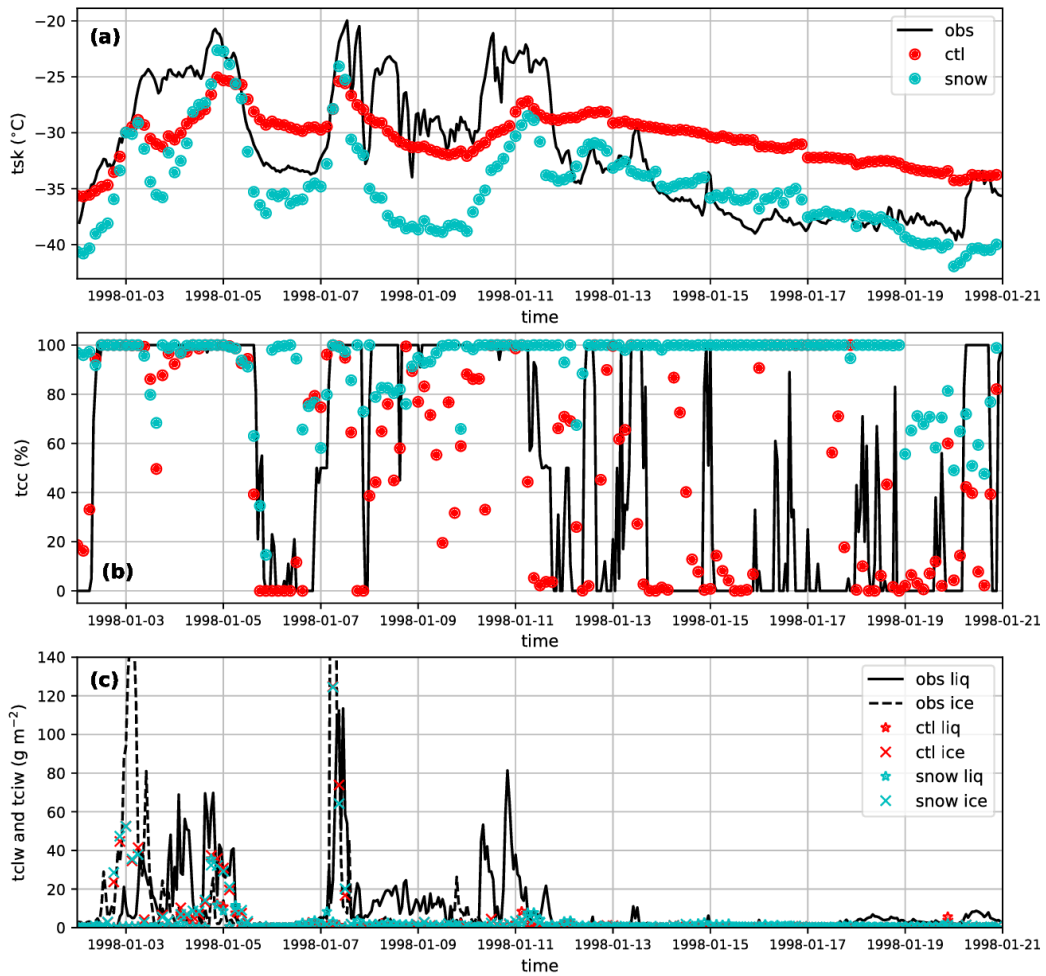


Figure 3.10: Concatenated day 2 ($t+24$ to $t+47$) forecasts for the period 1998-01-02 to 1998-01-20 of (a) skin temperature ($^{\circ}\text{C}$), (b) total cloud cover (tcc, %) and (c) total cloud liquid and ice water path from the coupled forecast experiments with bare sea ice (ctl, red dots) and with snow over sea ice (snow, cyan dots), compared to observations (obs, black lines).

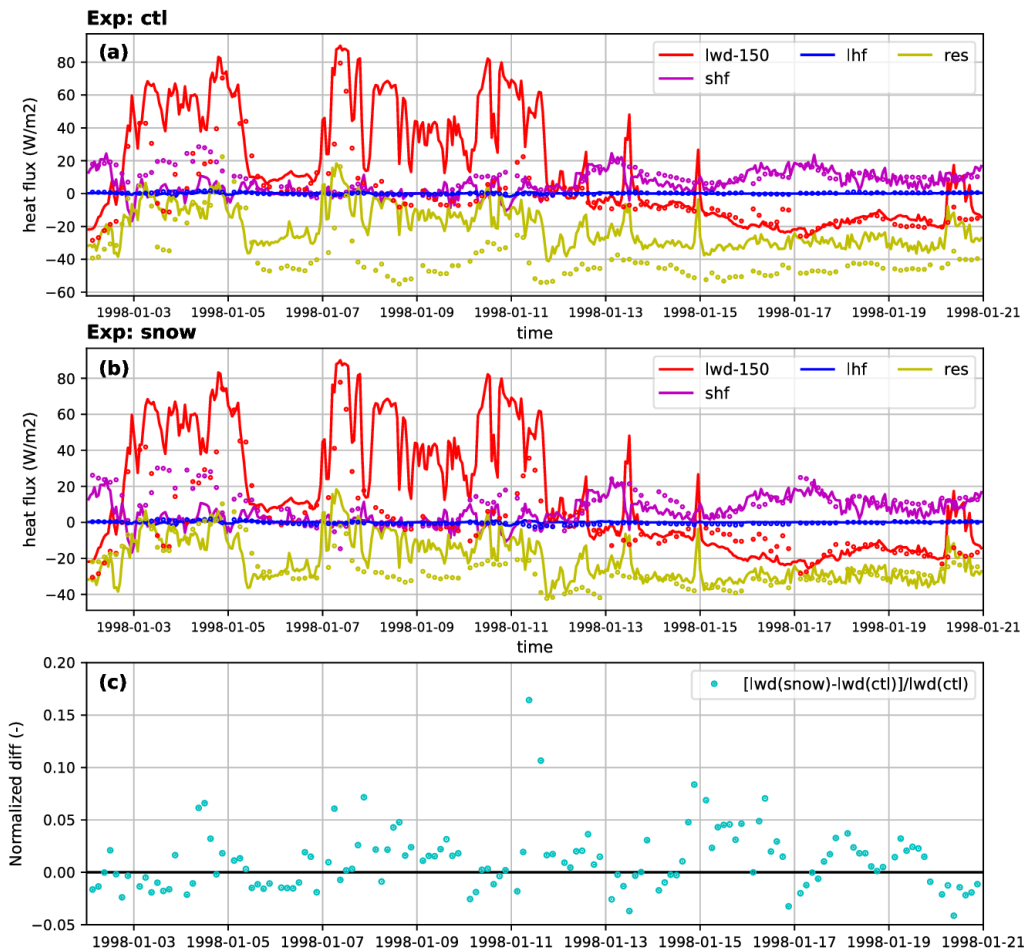


Figure 3.11: Concatenated day 2 ($t+24$ to $t+47$) forecasts for the period 1998-01-02 to 1998-01-20 of the surface downwelling longwave radiation (less 150 W m^{-2} , red), sensible and latent heat flux (magenta and blue, respectively) and the sum of the net radiation and sensible heat and latent heat fluxes (res, yellow), for (a) the *ctl* and (b) the *snow* experiments (symbols), compared to observations (continuous lines); (c) shows the normalized difference of the downwelling longwave radiative flux between *snow* and *ctl*, with respect to the one of *ctl*.

Day 2 ($t+24$ to $t+47$)			
Tskin	Bias	RMSE	Std dev
ctl	1.33	4.68	4.49
snow	-3.1	5.23	4.20
T10m	Bias	RMSE	Std dev
ctl	2.55	4.54	3.69
snow	-1.18	4.21	4.05

Table 3.1: Summary statistics (bias, root-mean-square-error and standard deviation of the error) for the analysed SHEBA period from 1998-01-01 to 1998-01-21 for model forecasts at a lead time of 2 days ($t+24$ to $t+47$ hours).

3.5 Impact of improved Arctic atmospheric boundary layer processes in IFS

The IFS single column model (SCM) was run for a period from the ASCOS 2008 field campaign in the Arctic Ocean. Figure 3.12 shows an example of the IFS SCM potential temperature profile for a decoupled stratocumulus boundary layer from ASCOS. The revised scheme (red) improves the structure of the boundary layer, with the surface mixed layer (capped by orange line) separated from the cloud mixed layer above by a stable layer. Note that in this case the stratocumulus cloud layer is not diagnosed by the original scheme.

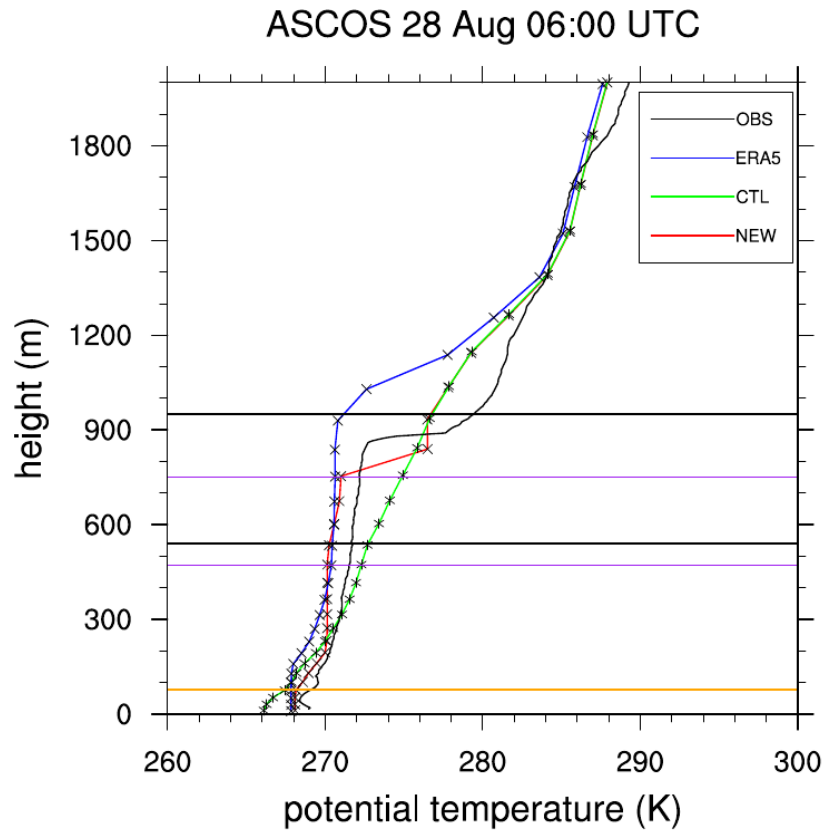


Figure 3.12: Potential temperature profile for a case from ASCOS, showing observations (black), ERA5 (blue), control case (green) and the new scheme (red). Horizontal black (purple) lines denote the cloud layer from observations (new scheme).

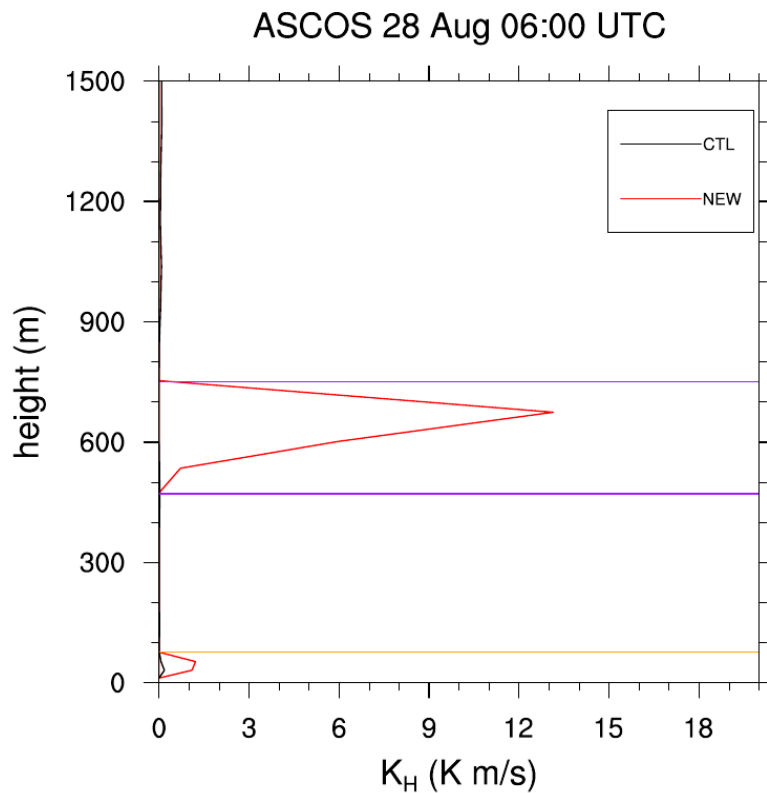


Figure 3.13: Eddy diffusivity profile for the control (black) and new scheme (red). Purple lines denote the cloud layer and the orange line the top of the surface mixed layer.

The eddy diffusivity profile for this case is shown in Figure 3.13, for the original (black) and new (red) scheme. The increased eddy diffusivity within the cloud layer (denoted by purple lines) in the new scheme promotes the mixed layer above the surface layer (shown in Figure 3.12), in contrast to the stable profile of the control case. The lack of cloud in the control case cools the surface relative to the observations.

Table 3.2 summarises the root mean square error (RMSE) for various parameters averaged over the model timestep relative to the observations for a 5-day period from ASCOS. The model was run for multiple 24-hour periods using initial conditions from ERA5, for a total of 10 simulations.

	Control	New
Temperature lowest model level (11.5 m) (°C)	1.69	1.69
Downwelling LW at surface (W/m ²)	37.4	30.1
Liquid water path (g/m ²)	67.7	64.8
Cloud top height (m)	509	343
Cloud depth (m)	608	385

Table 3.2: Summary of the RMSE for various parameters over a 5-day period from ASCOS for the control case and new scheme.

The revised scheme improves the RMSE for cloud and radiative properties for the ASCOS Arctic stratocumulus case, including the downwelling long-wave (LW) radiative flux at the surface, the liquid water path, and the cloud top height and cloud depth. The RMSE of the temperature in the lowest model level is unchanged for this case.

4. CONCLUSIONS AND OUTLOOK

The APPLICATE project contributes to improving the simulation and prediction of Arctic changes on daily to centennial timescales. Such model improvement requires an assessment of model deficiencies, development of new schemes to complement or correct the existing models and a thorough assessment of their performance in a variety of contexts and applications. This deliverable focuses on the evaluation on timescales of a few days of the impact of: 1. the inclusion of dynamical and/or thermodynamic sea ice models in numerical weather prediction systems, 2. the extension of single-layer snow schemes on land to multi-layer snow schemes, 3. the inclusion of snow schemes on top of sea ice, 4. an improved version of the eddy-diffusivity mass-flux scheme which detects decoupled stratocumulus.

The 1-dimensional GELATO-1D sea ice model has been implemented and tested within the ARPEGE/AROME forecast systems whereas the LIM2 dynamic and thermodynamic sea ice model was tested within the IFS prediction system. The evaluation was carried out against observational data collected at stations in the framework of the Year of Polar Prediction for ARPEGE/AROME and against the OCEAN5 analysis for IFS. An interactive sea ice model leads to a robust increase in forecast quality for near-surface temperature close to the sea ice edge in the ARPEGE/AROME prediction system. Bias and standard deviation are simultaneously substantially reduced. The temperature gradient across the sea ice edge is more realistic. Exploiting both observed sea surface temperatures and sea ice fraction to initialize the model is essential to optimize the benefits from the interactive sea ice model. Similarly, extracting boundary conditions from a global model which also uses an interactive sea ice model improves substantially the performance of the regional prediction system.

The dynamic coupling of the ice cover in IFS allows for capturing accurately rapid changes in sea ice concentration, especially along the sea ice edge as illustrated on a case study. The use of a dynamic sea ice model in high-resolution weather forecasts generally improves sea ice predictions at typical numerical weather prediction time scales, which in turn has repercussions on local 2-metre temperature forecasts. A substantial impact is seen onto the near surface temperature (up to 6°C) when the large-scale meteorological situation is favourable. The impact on large-scale atmospheric forecast performance is mostly neutral though.

The evaluation of a multi-layer snow scheme of intermediate complexity (following the definition by Boone & Etchevers, 2001), introduced into IFS prediction system has been carried out over the ESM-SnowMIP sites and in global offline simulations. It demonstrated the added value of this new scheme for the representation of snow depth and snow water equivalent (SWE). Mean (over all ESM-SnowMIP sites) normalized root-mean-square-error (NRMSE) of snow depth is reduced by more than 30% both in wintertime and springtime, whereas for SWE is reduced by about 9% and 12.5% during wintertime and springtime, respectively. The evaluation of global offline simulations using the surface SYNOP network over multiple years confirms the results at the sites at a broader spatial scale. In global coupled forecasts (in IFS), the multi-layer snow scheme improves the simulation 2-metre temperature at forecast day 2 during very cold episodes throughout the season at the Sodankylä site. It also increases the amplitude of the diurnal cycle by approximately 1°C, mainly associated to reduced warm bias at the daily minimum compared with the previous single-layer scheme. The evaluation of global coupled ten-day forecasts over the Arctic in the winter season, reported in D2.5, D5.3 and Arduini et al. (2019), confirm the improvements in the simulation of the daily minimum 2-metre temperature at different lead times.

Including this multi-layer snow scheme over sea ice in the IFS prediction system allows for a marginally better simulated temperature in the lower atmosphere for a case study from the SHEBA campaign. This case-study demonstrated the importance of accounting for snow presence and highlighted the impact of compensating errors among processes in the Arctic surface energy balance. When the cloud radiative forcing is correctly simulated by the model, the multi-layer snow scheme improves the simulation of the skin temperature. This is mainly associated with the reduction of the heat flux from the underneath ice to the surface. However, an underestimation of clouds' liquid water in the model during the analysed time period, induced errors in the cloud radiative forcing. Clouds errors combined with a more rapid surface cooling for the simulation with the snow over sea ice increase the RMSE of skin temperature compared to the one without snow.

A revised version of the eddy-diffusivity mass-flux scheme was proposed to identify decoupled stratocumulus in the IFS prediction system. This scheme detects and simulates cloud layers which would not have been represented before, as seen in an ASCOS Arctic stratocumulus case. The root mean square error for clouds and radiative properties are drastically reduced with this improved scheme for this case study.

Based on these results, this deliverable also intends to provide recommendations and guidance for the next generation of numerical weather prediction systems. Introducing an interactive sea ice model, even only a thermodynamic one, is sufficient to obtain robust improvements in forecast quality along the sea ice edge. We therefore conclude that better weather predictions could be achieved in the polar regions in the future with a generalization of the use of interactive sea ice models in operational weather prediction systems. Substantial improvements in the representation of cold events at high latitudes are also robust with the introduction of a multi-layer snow scheme over land. Therefore, we conclude that multi-layer snow schemes should be implemented in operational weather prediction systems to correctly represent snow processes occurring at different time scales, from (sub) daily to seasonal, and improve the simulation of the diurnal cycle of 2-metre temperature in the Arctic region. However, the results here presented must be confirmed in data assimilation experiments, in which the information from one forecast is propagated to the following.

Regarding the use of multi-layer snow models on ice, our recommendations would be more cautious since those developments may only be fully beneficial if model errors due to other processes, such as

cloud cover or properties, are also reduced. Indeed, we observed that such a snow model can act as an amplifier of previously existing errors in skin temperature during periods of liquid-phase cloud cover.

Finally, the revised version of the eddy-diffusivity mass-flux scheme showed highly promising results in detecting and simulating decoupled stratocumulus layers. However, a more extensive evaluation in short-term forecasts would be required to provide robust recommendations regarding its use in an operational mode.

5. REFERENCES

- Arduini, G., Balsamo, G., Dutra, E., Day, J., Sandu, I., Boussetta, S., & Haiden, T. (2019). Impact of a multi-layer snow scheme on near-surface weather forecasts. *Journal of Advances in Modeling Earth Systems*, Submitted.
- Balsamo, G., Albergel, C., Beljaars, A., Boussetta, S., Brun, E., Cloke, H., ... Vitart, F. (2015). ERA-Interim/Land: A global land surface reanalysis data set. *Hydrology and Earth System Sciences*, 19(1), 389–407. <https://doi.org/10.5194/hess-19-389-2015>
- Balsamo, Gianpaolo, Viterbo, P., Beljaars, A., van den Hurk, B., Hirschi, M., Betts, A. K., & Scipal, K. (2009). A revised hydrology for the ECMWF model: Verification from field site to terrestrial water storage and impact in the integrated forecast system. *Journal of Hydrometeorology*, 10(3), 623–643. <https://doi.org/10.1175/2008JHM1068.1>
- Boone, A., & Etchevers, P. (2001). An Intercomparison of Three Snow Schemes of Varying Complexity Coupled to the Same Land Surface Model: Local-Scale Evaluation at an Alpine Site. *Journal of Hydrometeorology*, 2, 374–394.
- Burke, E. J., Dankers, R., Jones, C. D., & Wiltshire, A. J. (2013). A retrospective analysis of pan Arctic permafrost using the JULES land surface model. *Climate Dynamics*, 41(3–4), 1025–1038. <https://doi.org/10.1007/s00382-012-1648-x>
- Decharme, B., Brun, E., Boone, A., Delire, C., Le Moigne, P., & Morin, S. (2016). Impacts of snow and organic soils parameterization on northern Eurasian soil temperature profiles simulated by the ISBA land surface model. *Cryosphere*, 10(2), 853–877. <https://doi.org/10.5194/tc-10-853-2016>
- Dee, D. P., Uppala, S. M., Simmons, A. J., Berrisford, P., Poli, P., Kobayashi, S., ... Vitart, F. (2011). The ERA-Interim reanalysis: Configuration and performance of the data assimilation system. *Quarterly Journal of the Royal Meteorological Society*, 137(656), 553–597. <https://doi.org/10.1002/qj.828>
- Dutra, E., Balsamo, G., Viterbo, P., Miranda, P. M. A., Beljaars, A., Schar, C., & Elder, K. (2010). An improved snow scheme for the ECMWF land surface model: Description and offline validation. *Journal of Hydrometeorology*, 11(4), 899–916. <https://doi.org/10.1175/2010JHM1249.1>
- Dutra, E., Viterbo, P., Miranda, P. M. A., & Balsamo, G. (2012). Complexity of snow schemes in a climate model and its impact on surface energy and hydrology. *Journal of Hydrometeorology*, 13(2), 521–538. <https://doi.org/10.1175/JHM-D-11-072.1>
- Donlon, C. J., M. Martin, J. D. Stark, J. Roberts-Jones, E. Fiedler and W. Wimmer (2011). The Operational Sea Surface Temperature and Sea Ice analysis (OSTIA). *Remote Sensing of the Environment*. doi: 10.1016/j.rse.2010.10.017.
- Essery, R., Kontu, A., Lemmetyinen, J., Dumont, M., & Ménard, C. B. (2016). A 7-year dataset for driving and evaluating snow models at an Arctic site (Sodankylä, Finland). *Geoscientific Instrumentation, Methods and Data Systems*, 5(1), 219–227. <https://doi.org/10.5194/gi-5-219-2016>
- Fichefet, T., & Maqueda, M. A. M. (1997). Sensitivity of a global sea ice model to the treatment of ice thermodynamics and dynamics, 102.
- Grenfell TC, Maykut GA (1977). The Optical Properties of Ice and Snow in the Arctic Basin. *J Glaciol*. doi: 10.3189/S0022143000021122
- Haiden, T., Sandu, I., Balsamo, G., Arduini, G., & Beljaars, A. (2018). Addressing biases in near-surface forecasts | ECMWF. *ECMWF Newsletter*, (157). <https://doi.org/10.21957/eng71d53th>
- Holtstlag, A. A. M., Svensson, G., Baas, P., Basu, S., Beare, B., Beljaars, A. C. M., ... Van De Wiel, B. J. H. (2013). Stable atmospheric boundary layers and diurnal cycles: Challenges for weather and climate models. *Bulletin of the American Meteorological Society*, 94(11), 1691–1706. <https://doi.org/10.1175/BAMS-D-11-00187.1>

- Hunke, E.C. and Lipscomb, W.H.. 2010. CICE: the Los Alamos sea ice model, documentation and software user's manual, Version 4.1 (Tech. Rep. LA-CC-06-012). Los Alamos, NM: Los Alamos National Laboratory.
- Jin, J., Gao, X., Yang, Z.-L., Bales, R. C., Sorooshian, S., Dickinson, R. E., ... Wu, G. X. (1999). *Comparative Analyses of Physically Based Snowmelt Models for Climate Simulations*.
- Keeley, S., & Mogensen, K. (2018). Dynamic sea ice in the IFS. *ECMWF Newsletter No. 156*, (156), 23–29. <https://doi.org/10.21957/4ska25furb>
- Krinner, G., Derksen, C., Essery, R., Flanner, M., Hagemann, S., Clark, M., ... Zhu, D. (2018). ESM-SnowMIP: Assessing snow models and quantifying snow-related climate feedbacks. *Geoscientific Model Development*, 11(12), 5027–5049. <https://doi.org/10.5194/gmd-11-5027-2018>
- Køltzow, M., Casati, B., Bazile, E., Haiden, T., & Valkonen, T. (2019). An NWP Model Intercomparison of Surface Weather Parameters in the European Arctic during the Year of Polar Prediction Special Observing Period Northern Hemisphere 1. *Weather and Forecasting*, 34(4), 959–983.
- Le Moigne et al., Surfex v8.1 scientific documentation (2018). Available on : https://www.umr-cnrm.fr/surfex/IMG/pdf/surfex_scidoc_v8.1.pdf
- Leppänen, L., Kontu, A., Hannula, H.-R., Sjöblom, H., & Pulliainen, J. (2016). Sodankylä manual snow survey program. *Geosci. Instrum. Method. Data Syst*, 5, 163–179. <https://doi.org/10.5194/gi-5-163-2016>
- McPhee MG (1992). Turbulent heat flux in the upper ocean under sea ice. *J Geophys Res.* doi: 10.1029/92JC00239
- Ménard, C. B., Essery, R., Barr, A., Bartlett, P., Derry, J., Dumont, M., ... Wever, N. (2019). Meteorological and evaluation datasets for snow modelling at 10 reference sites: Description of in situ and bias-corrected reanalysis data. *Earth System Science Data*, 11(2), 865–880. <https://doi.org/10.5194/essd-11-865-2019>
- Miller, N. B., Shupe, M. D., Cox, C. J., Noone, D., Ola, P., Persson, G., & Steffen, K. (2017). Surface energy budget responses to radiative forcing at Summit, Greenland. *The Cryosphere*, 11, 497–516. <https://doi.org/10.5194/tc-11-497-2017>
- Morin, S., Lejeune, Y., Lesaffre, B., Panel, J. M., Poncet, D., David, P., & Sudul, M. (2012). An 18-yr long (1993-2011) snow and meteorological dataset from a mid-altitude mountain site (Col de Porte, France, 1325 m alt.) for driving and evaluating snowpack models. *Earth System Science Data*, 4(1), 13–21. <https://doi.org/10.5194/essd-4-13-2012>
- Notz D (2005). Thermodynamic and fluid-dynamical processes in sea ice. Ph.D. thesis, Univ. of Cambridge, Cambridge, U. K.
- Persson, O. G., Shupe, M. D., Perovich, D., & Solomon, A. (2017). Linking atmospheric synoptic transport, cloud phase, surface energy fluxes, and sea-ice growth: observations of midwinter SHEBA conditions. *Climate Dynamics*, 49, 1341-- 1364. <https://doi.org/10.1007/s00382-016-3383-1>
- Saha, S. K., Sujith, K., Pokhrel, S., Chaudhari, H. S., & Hazra, A. (2017). Effects of multilayer snow scheme on the simulation of snow: Offline Noah and coupled with NCEP CFSv2. *Journal of Advances in Modeling Earth Systems*, 9, 271–290. <https://doi.org/10.1002/2016MS000845>
- Salas y Méliá, D. (2002). A global coupled sea ice-ocean model. *Ocean Modelling* 4, 137-172.
- Voltaire, A., Saint-Martin, D., Sénési, S., Decharme, B., Alias, A., Chevallier, M., ... & Nabat, P. (2019). Evaluation of CMIP6 DECK Experiments With CNRM-CM6-1. *Journal of Advances in Modeling Earth Systems*, 11(7), 2177-2213.